

Figure 4.4: PL spectra of strained $\langle 110 \rangle$ Si/Si_{1-x}Ge_x/Si quantum wells measured at (a) 4K and (b)-(e) 77K. The dotted lines in (b)-(e) are the theoretical fitting of electron hole plasma model and the no-phonon component of the model. The onsets of the no-phonon lines at the low energy side are the bandgaps of the quantum wells, $E_{g,PL}$.

$\beta = 0$. The electron-hole plasma transitions then have a linear cut-off edge.

To model the shape from each possible electron-hole transition, the relative ratios of the different TO transitions (Si-Si, Si-Ge, Ge-Ge) were taken from the statistical bond counting model of Weber and Alonso [66], and the phonon energies of Ref. [66] were used. The lineshape due to each possible electron-hole transition was then convolved with Eqn. 4.1, which represents all possible electron-hole transitions. The three adjustable parameters in fitting the lineshape were the bandgap ($E_{g,PL}$), the ratio of the NP line strength to the total strength of TO lines (r_{np}), and the sum of $F_e + F_h$ (which affects the linewidth). The fitted spectra are shown in Fig. 4.4. Also shown in Fig. 4.4 were the contribution from the NP lines only. The bandgap, $E_{g,PL}$, is the lower edge of this component, and was found to be fairly insensitive to all of the other fitting parameters, and also insensitive to variations in the assumed relative strengths of the various TO transitions. A summary of the fitting results for different samples are shown in Table 4.2. Note that the bandgap value obtained from 77K PL of Fig. 4.4(b) is very close to the energy position of NP line (excitonic bandgap) in 4K PL (Fig.2(a)) of the same sample.

To determine the “true bandgap” of strained $\langle 110 \rangle$ $\text{Si}_{1-x}\text{Ge}_x$, we have to calculate the quantum confinement energies of both holes and electrons. We assumed a square potential profile, a theoretical valence band discontinuity $\Delta E_v = 0.71x$ [1], the measured quantum well thickness, the hole effective mass of $0.28 m_o$ [10], and the electron effective mass of $0.19 m_o$. The quantum confinement effect has been observed with Si/ $\text{Si}_{0.71}\text{Ge}_{0.29}$ /Si quantum wells with different well widths. Fig. 4.5 plots the excitonic bandgap from 4K PL vs well widths with the theoretical curve using these parameters. A quantum confinement energy up to 110 meV was observed by varying the well width from 133Å to 17Å.

Fig. 4.6 displays a plot of the bandgap of strained $\langle 110 \rangle$ $\text{Si}_{1-x}\text{Ge}_x$ versus Ge content after corrections for quantum confinement as well as the bandgap of strained

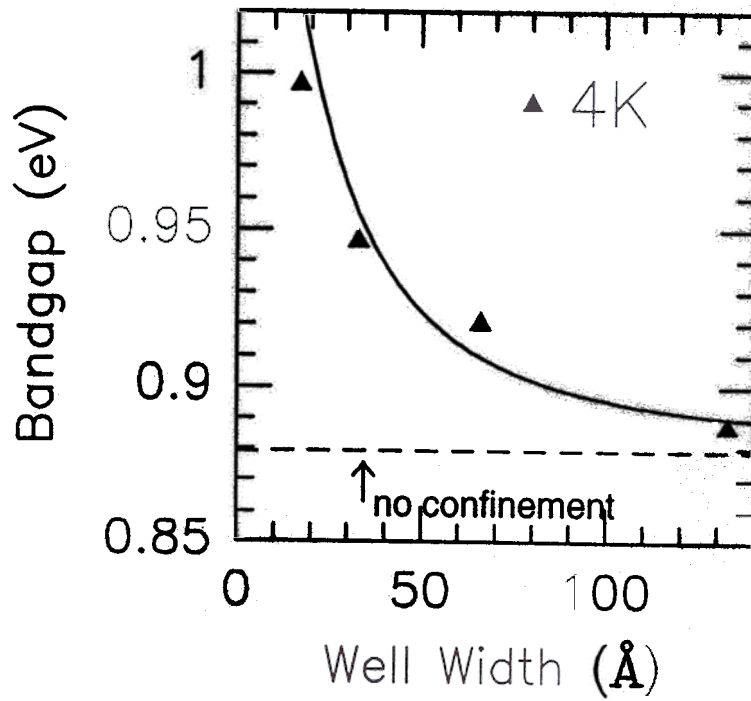


Figure 4.5: The quantum confinement shift measured by 4K PL. The solid line is the fitting using the assumptions described in text. The dotted line indicates the bandgap after quantum confinement correction.

$\langle 100 \rangle$ Si_{1-x}Ge_x layers after quantum confinement correction. The data is very close to the theoretical curve of People et al., which is plotted in Fig. 4.6 as well as the bandgap of relaxed Si_{1-x}Ge_x [66] for comparison. Although the bandgap of strained Si_{1-x}Ge_x on $\langle 110 \rangle$ substrates is predicted to be slightly lower than that on $\langle 100 \rangle$ substrates (approximately 15 meV lower for $x=0.4$ [29]), within experimental resolution of E_g and x , we can not observe such a shift in a comparison with the 77K PL of $\langle 100 \rangle$ and $\langle 110 \rangle$ samples grown in our lab as shown in Fig. 4.6.

4.4 Alloy scattering and conduction band offset

In this section, we will examine the strength of the no-phonon luminescence line, and show how its dependence on well width can be used to measure the conduction band offset. In the $\langle 110 \rangle$ strained layers, the integrated NP/TO ratio was substantially stronger than that observed in comparable $\langle 100 \rangle$ structures. For example, sample 1463 ($x=0.29$) had an NP/TO ratio, r_{np} , of 3.2, extracted from the PL spectrum at 77K. For a sample of similar composition on $\langle 100 \rangle$ substrates, we typically observed $r_{np} \sim 1.6$. In the 4K spectra (Fig. 4.4 (a)), the relative height of the NP line was also about twice that in similar $\langle 100 \rangle$ samples. Fig. 4.7 plots the fitted ratio of the NP line strength to the total strength of TO lines vs Ge fraction for both $\langle 110 \rangle$ and $\langle 100 \rangle$ samples at 77K, where impurity localization is not expected to affect the NP/TO ratio.

Note that the different data points for the same Ge concentration are due to different well widths. All the $\langle 100 \rangle$ samples have a thickness over 100 Å, for which a high NP/TO ratio would be expected (Fig. 4.9). It is obvious that $\langle 110 \rangle$ has higher ratios than $\langle 100 \rangle$ for all Ge compositions. The NP process is believed to arise solely from alloy scattering at 77K, which provides the momentum necessary for

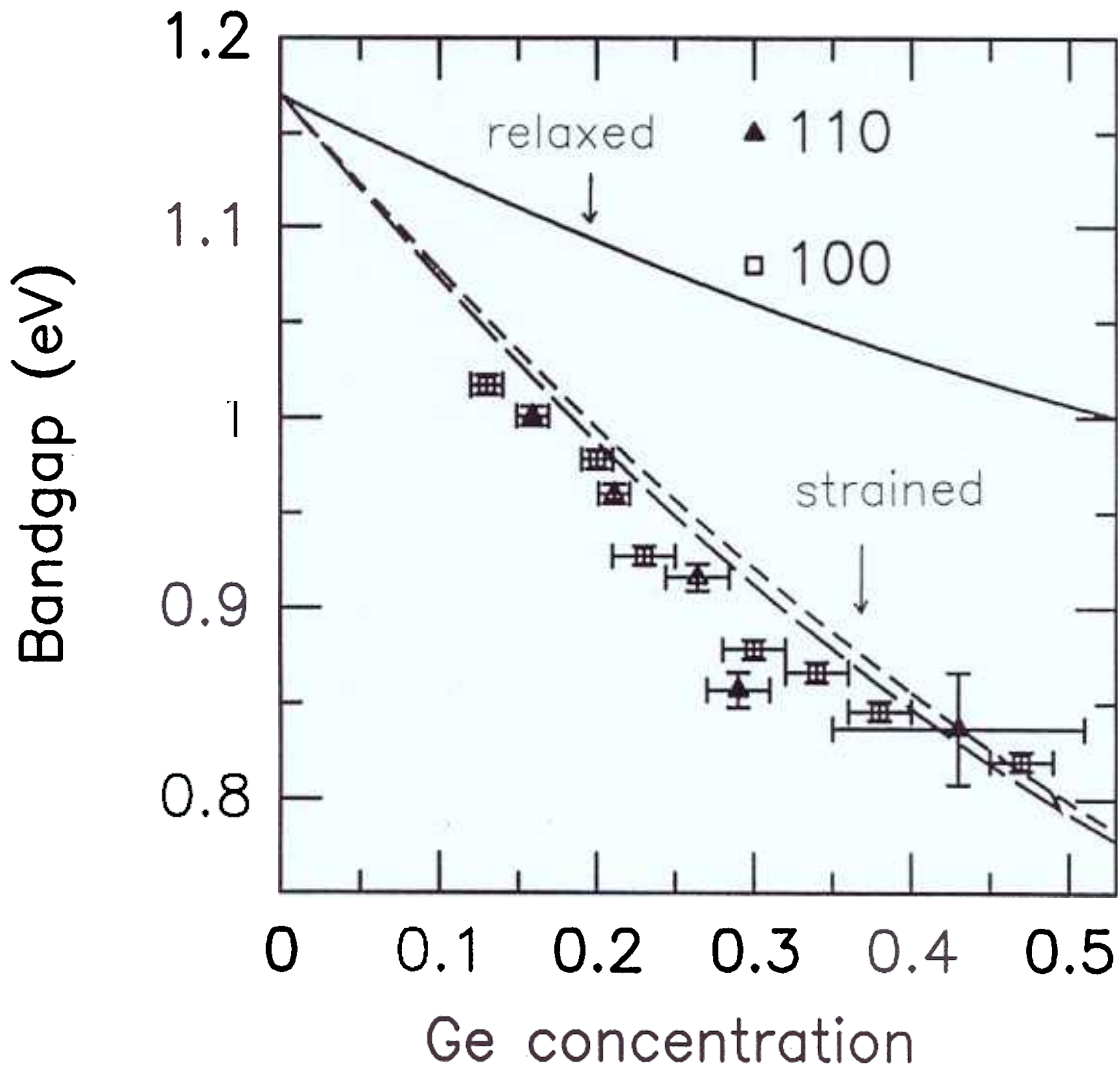


Figure 4.6: The plot of bandgap vs Ge concentration for both strained (110) and (100) $\text{Si}_{1-x}\text{Ge}_x$ alloys measured from 77K PL. The solid line is the relaxed bandgap. The upper dashed line is the prediction of People *et al.* for strained $\text{Si}_{1-x}\text{Ge}_x$ on Si (100) substrates and the lower is for (110) substrates.

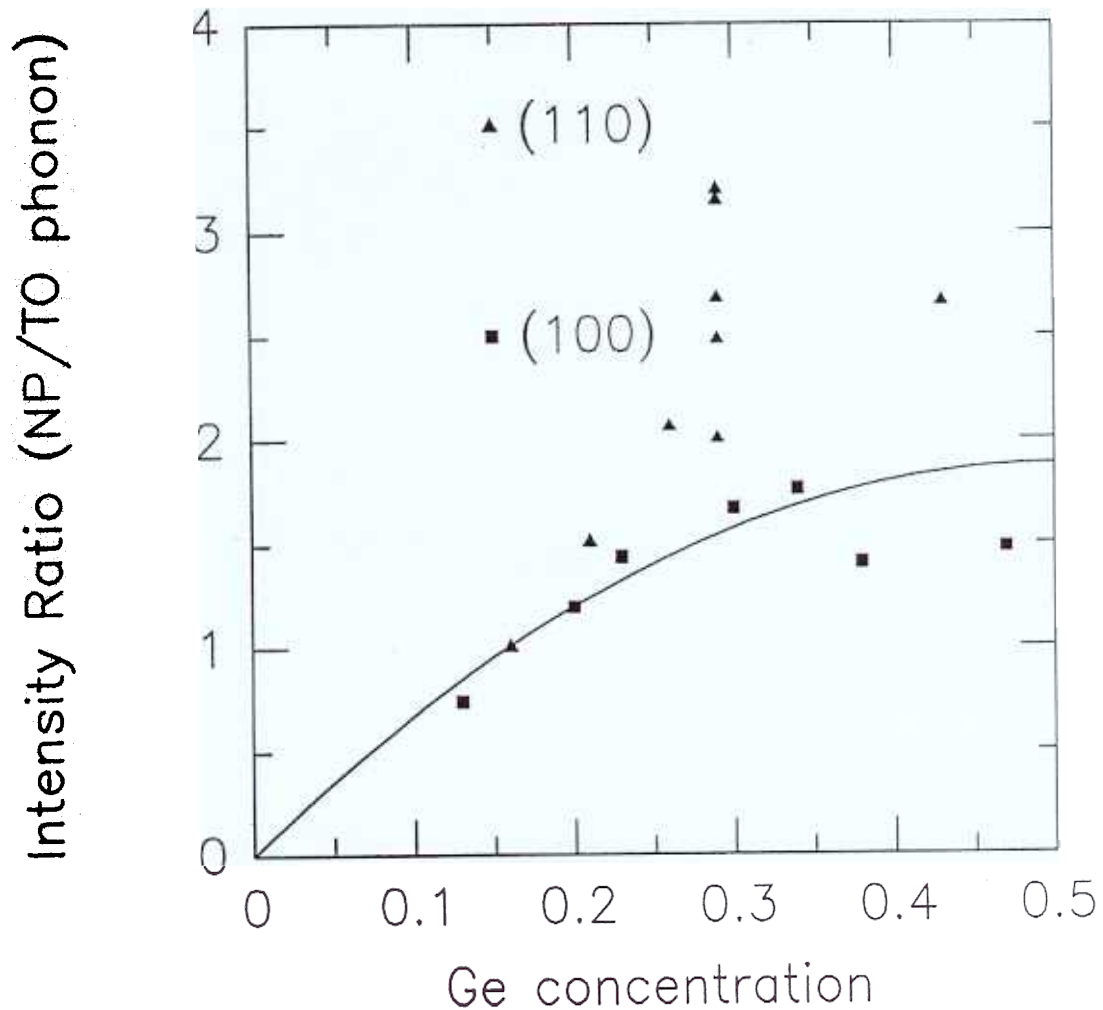


Figure 4.7: NP/TO ratio vs Ge concentration of strained (110) and (100) quantum wells. The (110) wells have higher ratios, compared to (100) wells. The solid line is the best fit of $x(1-x)$ dependence of (100) data. Note that the scattered points of (110) data are due to different well widths.

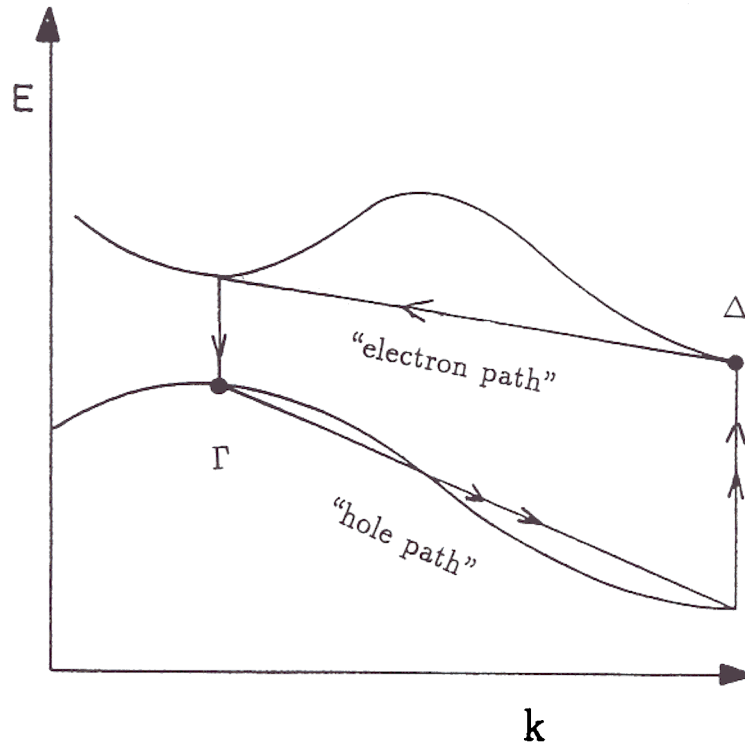


Figure 4.8: Schematic diagram of alloy scattering paths. The electron path consists of an electron being scattered from the Δ point to the Γ point of conduction band by alloy scattering, followed by subsequent recombination with a hole at Γ point. The hole path consists of a hole scattered from the Γ point to the Δ point of valence band, followed by subsequent recombination with an electron at the Δ point.

the recombination of the Δ electrons and Γ holes in the indirect bandgap $\text{Si}_{1-x}\text{Ge}_x$. In the no-phonon recombination process through the alloy scattering process, there are two paths for the recombination of electrons and holes [67] as shown in Fig. 4.8. They are

(a) an “electron path”: Δ electrons scattered from the Δ point to the Γ point of conduction band by alloy scattering, followed by subsequent recombination with holes at the Γ point.

(b) a “hole path”: holes scattered from Γ point to Δ point of valence band by alloy scattering, followed by subsequent recombination with electrons at the Δ point.

According to perturbation theory, the vertical transition rate of each path is proportional to the square of the inverse of vertical bandgap at each point. The vertical

bandgap at Δ point is larger than of that at the Γ point (taking $\text{Si}_{0.8}\text{Ge}_{0.2}$ as an example, $E_g(\Delta)=4.3$ eV, $E_g(\Gamma)=2.9$ eV, interpolated from the values of Si and Ge [68]). As a result, the transition rate through the electron path is two times of that through the hole path for $\text{Si}_{0.8}\text{Ge}_{0.2}$, if alloy scattering rates which introduce the intraband transitions are the same for holes and electrons. Recent evidence [55, 69] has shown that the hole alloy scattering potential was smaller than electron alloy potential, i.e., hole alloy scattering rate is smaller than electron alloy scattering rate. This effect further decreases the transition rate of hole path. Therefore, we will assume that the electron path is dominant in the following model of the alloy scattering rate versus quantum well width. We will justify the assumption later in this section.

The well width dependence of the NP/TO ratios at 77K for both < 110 > and < 100 > quantum wells is shown in Fig. 4.9. If the matrix element of phonon scattering is independent of well width, the NP/TO ratios can represent the relative alloy scattering rates.

The alloy scattering rate, R_{alloy} , is given most generally by Eqn. 109 in Ref.[70]. For a fixed Ge content x , the well width dependence of R_{alloy} can be simplified to:

$$R_{\text{alloy}} \sim \int_{\Omega_0} \psi^4 dx \quad (4.3)$$

where Ω_0 is the width of the $\text{Si}_{1-x}\text{Ge}_x$ alloy and ψ is the (normalized) electron wave function. The intuitive argument of the fourth power dependence is that the scattering rate is square of its matrix element which is proportional to the square of wavefunction if the alloy fluctuation is a short range potential (delta function like). Assuming an electron path for alloy scattering, the calculated relative alloy scattering rates vs well width for different Ge contents and conduction band offsets are also displayed in Fig. 4.9. Because a more concentrated wave function in a narrow well will be more sensitive to alloy fluctuations (due to a small number of atoms sampled by the wave function), the alloy scattering rate increases as either the well width decreases or

the conduction band offset increases. However, if the well width is extremely narrow and too small to confine the wave function, the wave function will spread into the Si barriers, and thus the alloy scattering rate starts to decrease. Note that the data from $\langle 110 \rangle$ quantum wells has a slight increase as the well width is decreased, and then decreases for the well width under 30 Å. This is qualitatively consistent with the above argument of the width dependence of alloy scattering. Also note that $\langle 100 \rangle$ data has only a gradual decrease as well width decreases and no increase, consistent with a very small band offset providing negligible confinement. From best fit of the data, we have ΔE_c of 40 meV and 10 meV for $\langle 110 \rangle$ Si_{0.71}Ge_{0.29} and $\langle 100 \rangle$ Si_{0.8}Ge_{0.2}, respectively. The fact that the theoretical curve does not fit the data quite well indicates the complicate nature of no-phonon process which also involves the photon emission process, not included in this simple model. However, it is very difficult to measure such small offsets by other methods such as modulation doped structures. Therefore, we tentatively attribute the relatively larger NP/TO ratios to the relatively larger conduction band offset on $\langle 110 \rangle$ substrates than that on $\langle 100 \rangle$ substrates. To the best of our knowledge, this is the first time that the well width dependence of no-phonon luminescence strength has been used to measure band offsets. Note that if the hole path were dominant, the relative alloy scattering rate would vary more than 2 times from the value of thick well to its peak value in the narrow wells due to the large valence band offset (200 meV). That this is not observed is strong evidence of a dominant electron path for alloy scattering as assumed.

Finally, in Fig. 4.10, we compare our extracted ΔE_c to the predictions of People *et al.* [71] with reasonable agreement. To the best of our knowledge, this is the first time that the ΔE_c of pseudomorphic SiGe on Si $\langle 100 \rangle$ or $\langle 110 \rangle$ substrates has been measured and also the first time that band offsets have been measured by the well width dependence of the no-phonon luminescence process in any material.

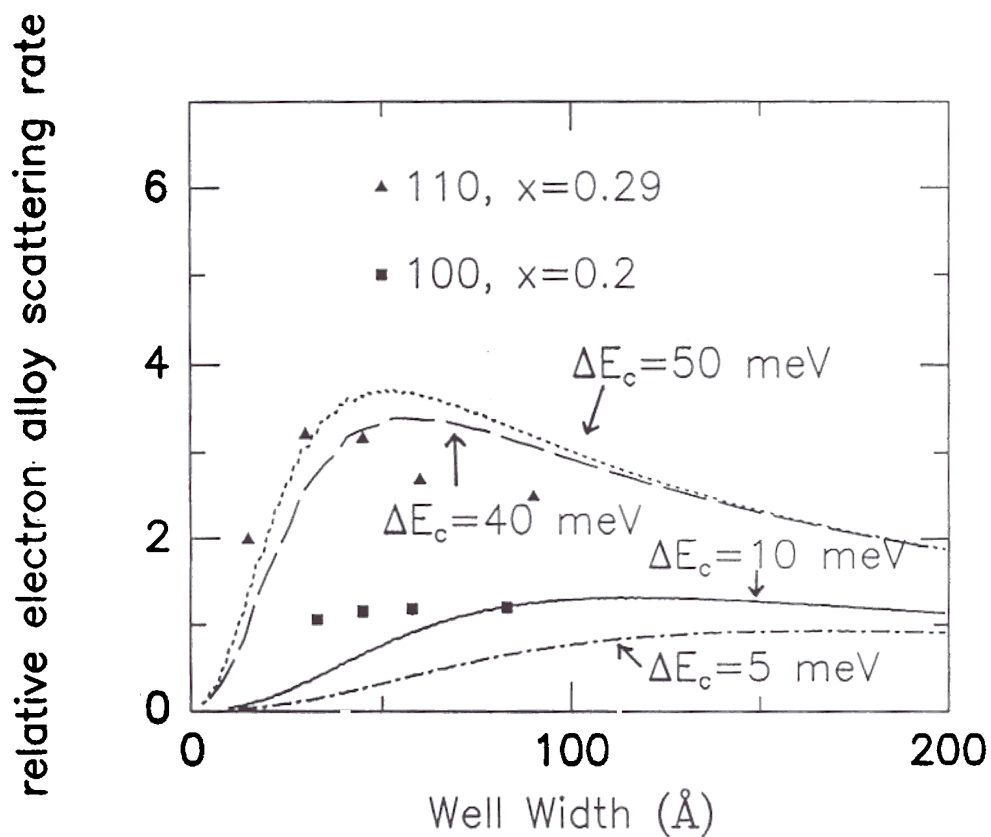


Figure 4.9: The NP/TO ratio vs well width for both (110) and (100) samples as well as the theoretical curves. The fitting of (110) data required a higher value of ΔE_c than that of (100) data.

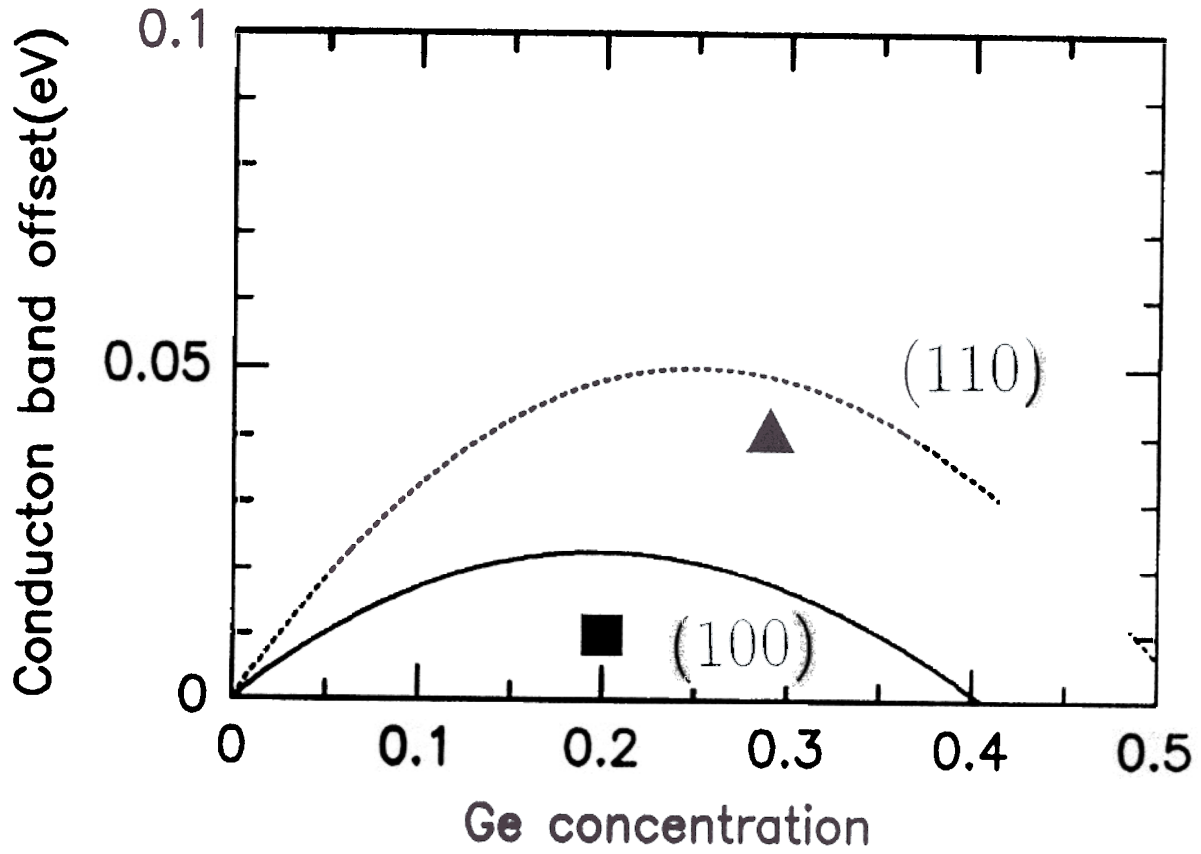


Figure 4.10: ΔE_c as a function of Ge content. The extracted ΔE_c data is compared to the prediction of People *et al.* [71].

4.5 Summary

We have reported the first growth of strained $\langle 110 \rangle$ $\text{Si}_{1-x}\text{Ge}_x$ by CVD, and we have used the photoluminescence spectroscopy to measure the bandgap of strained $\langle 110 \rangle$ $\text{Si}_{1-x}\text{Ge}_x$ on Si for the first time. Our results are in good agreement with the prediction of People et al. [72], but the small predicted difference between the bandgap of films strained on $\langle 110 \rangle$ vs $\langle 100 \rangle$ substrates has not been resolved within experimental error. The no-phonon luminescence of the $\langle 110 \rangle$ films is stronger than that on $\langle 100 \rangle$ substrates. Finally, a new technique for extracting the conduction band offsets was developed, and used to make the first measurement of ΔE_c in strained $\text{Si}_{1-x}\text{Ge}_x$ on Si substrates. It provided the evidence of the larger conduction band offset of strained $\text{Si}_{1-x}\text{Ge}_x$ on $\langle 110 \rangle$ substrates compared to that on $\langle 100 \rangle$ substrates.

Structural and Electrical Studies of Low-Temperature β SiC on Si

5.1 Introduction

The unique thermal and electronic properties of SiC make it a promising material for electronic and optoelectronic devices designed to operate in severe conditions such as high voltage, high temperature, high frequency, and high radiation. In the close-packed SiC structures, there are many different one-dimensional stacking polytypes. Those polytypes are similar in the two-dimensional close packed planes, but differ in the stacking sequence in the direction perpendicular to the two-dimensional planes. A repetitive ABC stacking sequence yields a zincblende structure. This is the only SiC polytype with cubic symmetry and is referred to as 3C or β -SiC (bandgap 2.2eV). The number 3 refers to the number of planes in the period and C refers to the cubic crystals. The other non-cubic crystals are referred to as the α -SiC family. This family includes a wide range of ordered, large period, stacked hexagonal (like 6H) or rhombohedral structures (15R). Among those polytypes, the substrates of 6H SiC (ABCCBA, bandgap 3 eV) are commercially available. The 6H SiC technologies are the most mature and its blue LEDs (light emitting diodes) ultraviolet photodetectors are currently commercially available (Cree Research, Inc). However, the light output is relative low ($13\mu W$ at 20 mA) due to the indirect bandgap of the SiC. Recently

5. Structural and Electrical Studies of Low-Temperature β SiC on Si 71

GaN based technology produced a double heterostructure LED with 1500 μ W at 20 mA [73], which is 2 orders of magnitude brighter than that of 6H SiC, hence replacing the SiC LED market share. However, the other advantages of SiC such as high temperature operation, very low leakage current, high thermal conductivity as well as the high values of electron saturation velocity (2×10^7 cm/sec) still make SiC highly competitive for potential device applications in extremely severe conditions.

Most of research activity of SiC is focused on 6H SiC, because of the maturity of bulk crystal growth technologies [74, 75, 76]. However, the high cost of the 6H SiC wafer (2,000 U.S. dollars per square inch) prevents its widespread application. There are no suitable substrates of 3C SiC crystals, but 3C SiC has been grown in the past on Si (100) substrates, despite 20 % mismatch of lattice constants and 8 % mismatch of thermal expansion coefficients between 3C SiC and Si.

Conventionally, the CVD growth of 3C SiC on Si requires high growth temperatures ($\geq 1300^\circ\text{C}$) [77] using separate precursors such as SiH_4 for Si and C_3H_8 for C, and an initial surface carbonization step [78, 79], which prevents the possibility of integration with silicon-based devices. Furthermore, the low material quality is reflected in very leaky Schottky barriers with a highest reported soft breakdown of only 8 - 10 V [80]. In this study, we report growth properties of cubic SiC on (100) Si grown at temperature as low as 700°C using a single gas precursor methylsilane without the carbonization step (first demonstrated by I. Golecki *et al.* [81]) and fabrication of the first Schottky diodes with avalanche breakdown on 3C SiC on Si.

5.2 Growth and characterization

Due to the lack of suitable 3C SiC substrates, 3C SiC was grown on Si (100) substrates. The SiC films were deposited on tilted (4° towards $\langle 110 \rangle$) and not-tilted Si substrates (10 cm in diameter) in our RTCVD reactor at a growth tem-

5. Structural and Electrical Studies of Low-Temperature β SiC on Si 72

perature of 700–1100°C. The growth pressure was 1 torr with a 1.5 sccm methylsilane (SiCH_3) flow and a 500 sccm hydrogen flow. As mentioned in section 2.4, the growth temperature (700–800°C) was accurately determined by the infrared transmission technique. Growth temperatures higher than 800°C were controlled by the tungsten-halogen lamp power which was previously calibrated with a thermocouple welded onto a Si wafer. The SiC thickness was measured by fitting the optical reflection spectra from 500 to 700 nm with the SiC index of refraction of 2.6. Since the temperature is not uniform across the wafer (the edge is about 50 °C lower than center), the thickness was measured at the spot very close to the position where the temperature was monitored (near the center of the wafer). Fig. 5.1 gives the Arrhenius plot of the growth rate of SiC on not-tilted (100) Si. The growth rate in the range 700–800°C varied exponentially with the inverse of temperature and the activation energy for this reaction-limited growth was 3.6 eV. This is higher than that of pure silicon growth (~ 2 eV) and may reflect the strong C–H bond. At higher growth temperature (800–1100°C), the growth rate had a weak temperature dependence, indicating mass-transport limited growth.

The crystallinity of the films was studied by XRD (X-ray diffraction) and TEM (transmission electron microscopy, in collaboration with E. A. Fitzgerald of ATT Bell Labs, P. Pirouz, J. W. Yang of Case Western Reserve Univ, and M. Sarikaya, M. Qian of Princeton Univ.). For the films grown at 750°C (sample 1182), the XRD spectrum of a 80nm film on not-tilted substrates exhibited a single crystalline feature with a broad unresolved $\text{CuK}_{\alpha 1}$ and $\text{CuK}_{\alpha 2}$ (400) peak (FWHM of 2θ is about 1.6°). The spectrum is shown in Fig. 5.2(a). But the TEM diffraction pattern (Fig. 5.2(b)) of the same sample showed evidence of some slightly in-plane rotated textures and very fine spots in the $\langle 110 \rangle$ direction. This indicates the poor crystallinity of the 750 °C films.

The crystallinity can be improved by increasing the growth temperature to 800°C

5. Structural and Electrical Studies of Low-Temperature β SiC on Si 73

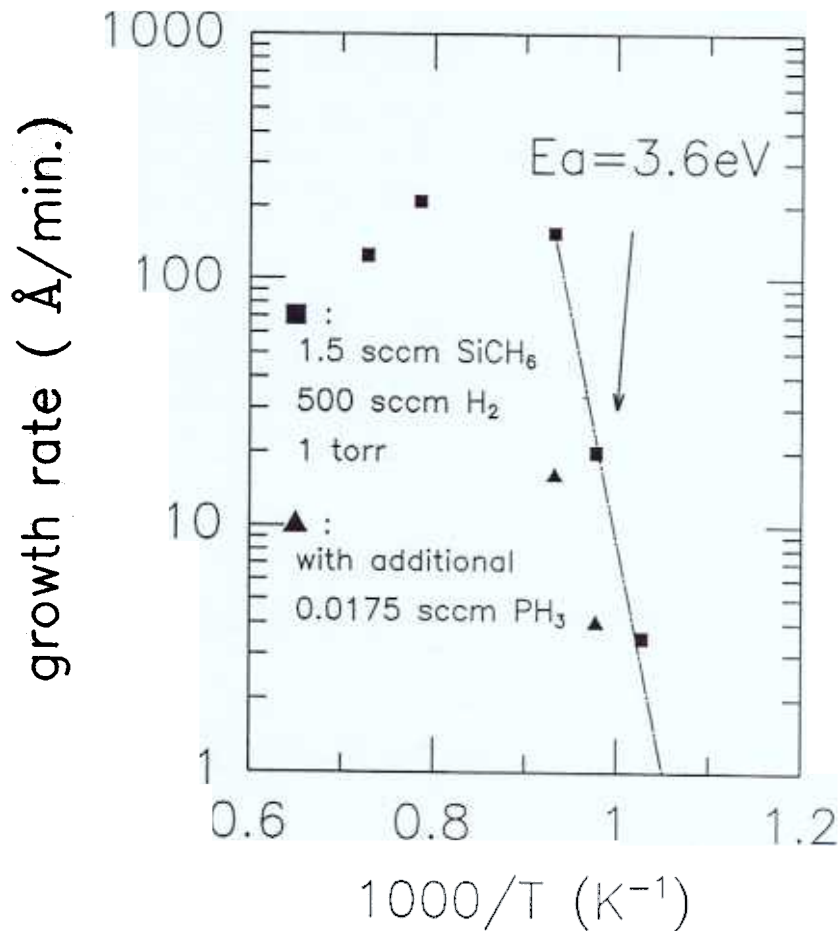


Figure 5.1: Arrhenius plot of the growth rate of SiC on not-tilted (100) Si. The growth in the range 700–800°C varied exponentially with the inverse of temperature and the activation energy for this reaction-limited growth was 3.6 eV. At higher growth temperature (800–1100°C), the growth rate had a weak temperature dependence, indicating mass-transport limited growth. Note that the addition of PH₃ decreased the growth rate.

5. Structural and Electrical Studies of Low-Temperature β SiC on Si 74

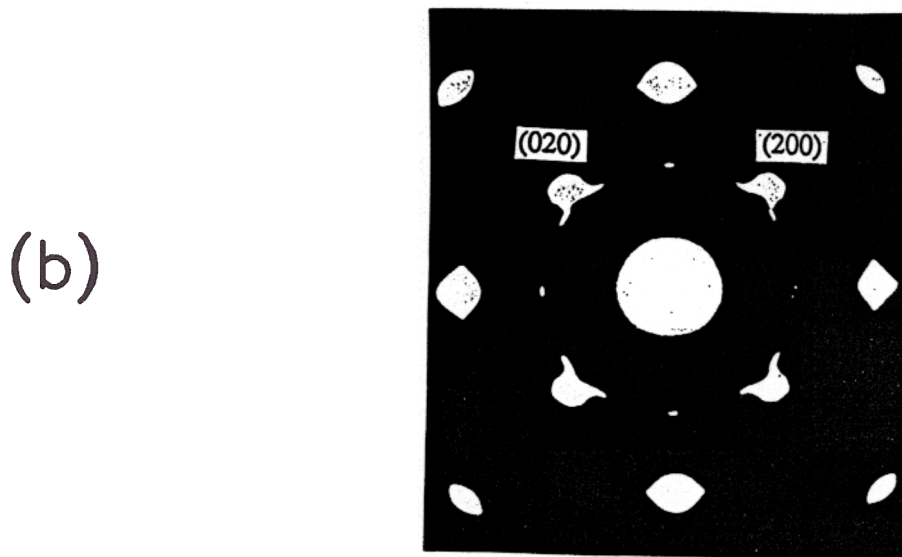
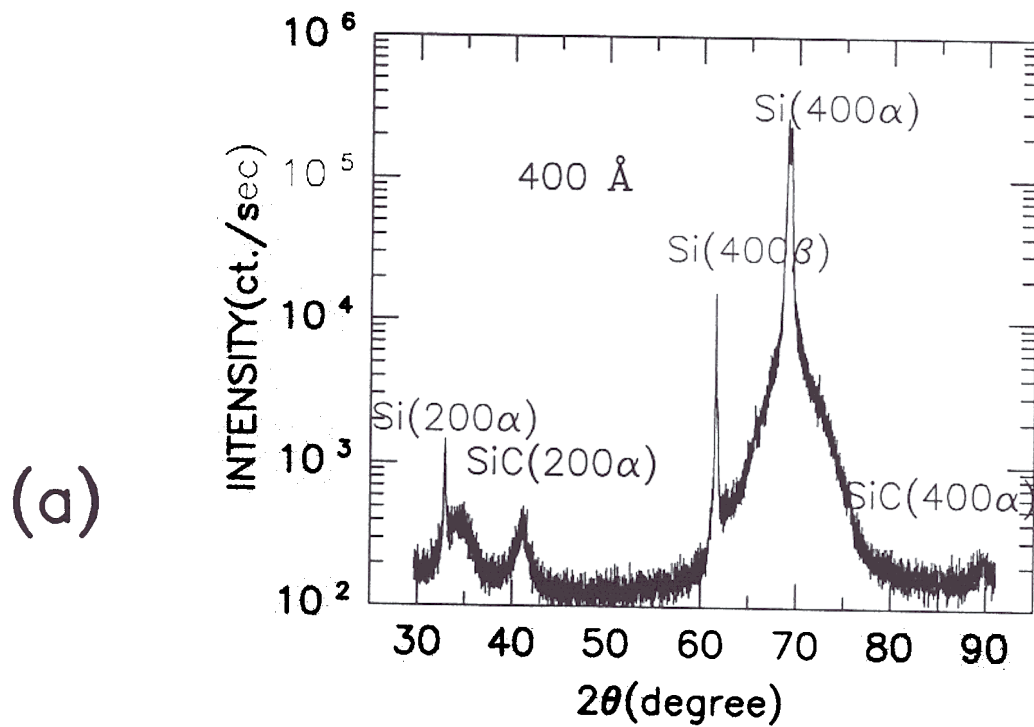


Figure 5.2: The XRD spectrum (a) and TEM diffraction pattern (b) of a 750°C-grown film. The XRD spectrum exhibited a single crystalline feature with a broad unresolved $\text{CuK}\alpha_1$ and $\text{CuK}\alpha_2$ (400) peak (FWHM of 2θ is about 1.6°). But the diffraction showed evidence of some slightly in-plane rotated textures and very fine spots in the $\langle 110 \rangle$ direction. This indicates the bad crystallinity of the 750 °C films.

5. Structural and Electrical Studies of Low-Temperature β SiC on Si 75

The XRD spectrum of a 0.3 μm SiC film grown at 800 °C (Fig. 5.3(a)) on not-tilted substrates showed that the FWHM of unresolved $\text{CuK}\alpha$ (400) peak was as small as 0.75°, which was similar to the value (0.65 – 0.7°) of 0.3 μm commercial (100) SiC on Si. The TEM diffraction pattern also displayed a well-defined single crystalline feature (5.3(b)). The films grown at 800 °C on tilted substrates had similar XRD spectra and TEM diffraction patterns, but had a smoother surface morphology, which facilitated the Schottky barrier fabrication. According to P. Pirouz, TEM also showed very high densities of stacking faults and dislocations, similar to the films of similar thickness grown by conventional high temperature growth techniques.

The Fourier transform infrared (FTIR) spectra (Fig. 5.4) of a 0.3 μm 800°C grown film on not-tilted substrates (sample 1183) displayed an absorption peak at 796 cm^{-1} (TO phonon absorption) with a FWHM of 50 cm^{-1} , which is similar to that of the films grown by conventional high temperature growth methods [82].

The Raman spectrum (Fig. 5.5) of the same sample (1183) showed a broad peak at 960 cm^{-1} with FWHM of 60 cm^{-1} , which is about 10 cm^{-1} below the LO phonon shift ($\sim 970 \text{ cm}^{-1}$) and probably correlated with the interface defects between SiC and Si [83].

The XRD spectrum of the films grown at 1000 °C and 1100 °C under the same gas conditions, however, indicated extra (111) and (220) peaks, indicating the growth of polycrystalline material. Therefore, the 800 °C is the optimum temperature for the single crystalline material growth. However, “two step growth,” namely, a thin layer grown at 800 °C first, followed by high temperature growth, again yielded single crystalline films. For example, a film with a thickness of 0.45 μm grown at 1000 °C formed a polycrystalline structure as determined by XRD (Fig. 5.6(a)). However, if a 0.15 μm layer was deposited at 800 °C, followed by a 0.3 μm film grown at 1000 °C this led to single crystalline growth at 1000 °C again (Fig. 5.6(b), sample 1289). This shows that a low temperature (800 °C) growth on the Si surface is essential for

5. Structural and Electrical Studies of Low-Temperature β SiC on Si 76

800°C FILMS : XRD, TEM

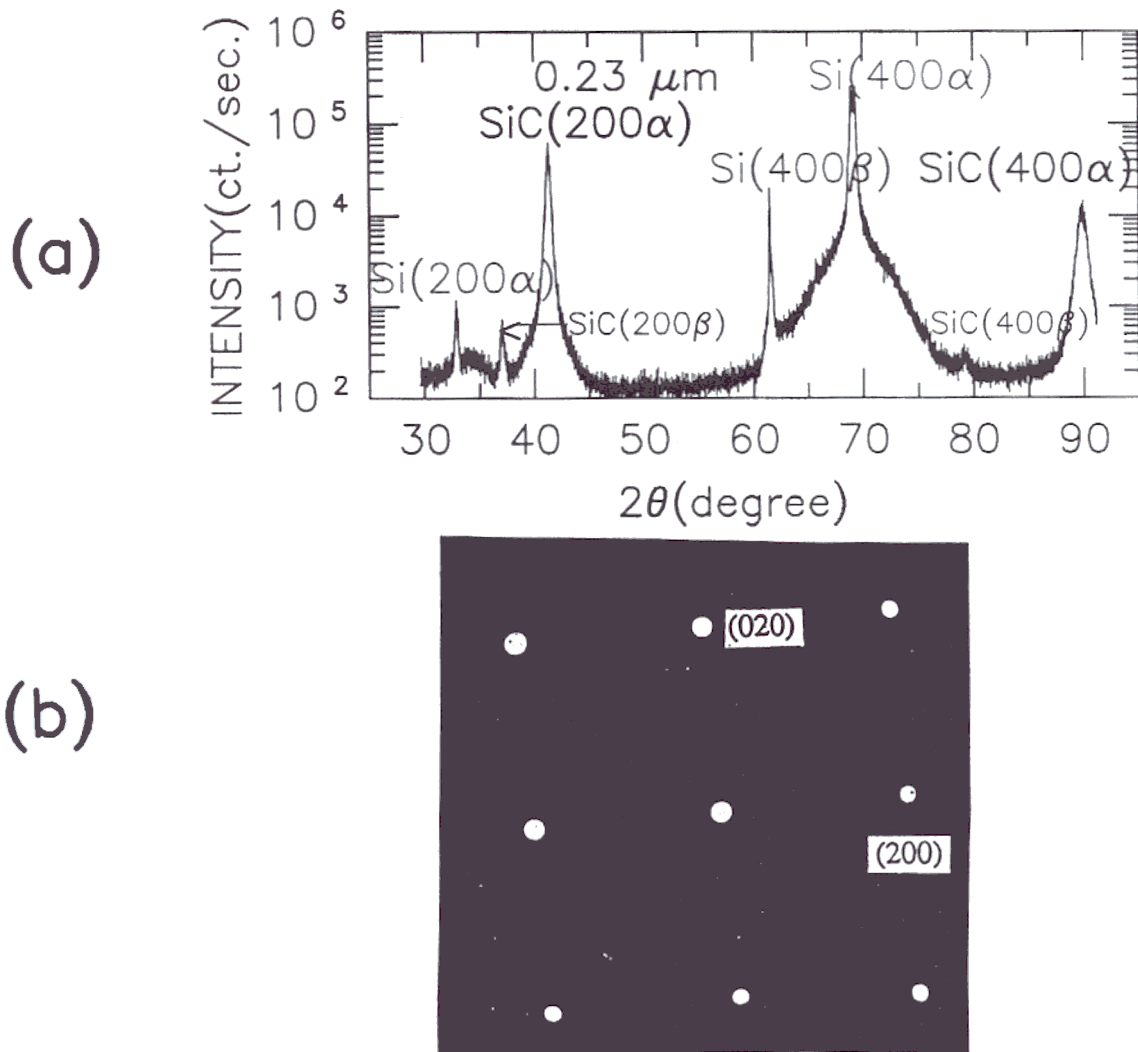


Figure 5.3: The XRD spectrum (a) and TEM diffraction pattern (b) of a 800°C-grown film. The XRD spectrum exhibited a single crystalline feature with a unresolved $\text{CuK}_{\alpha 1}$ and $\text{CuK}_{\alpha 2}$ (400) peak (FWHM of 2θ is as small as 0.75°). The TEM diffraction pattern also displayed a well-defined single crystalline feature.

5. Structural and Electrical Studies of Low-Temperature β SiC on Si 77

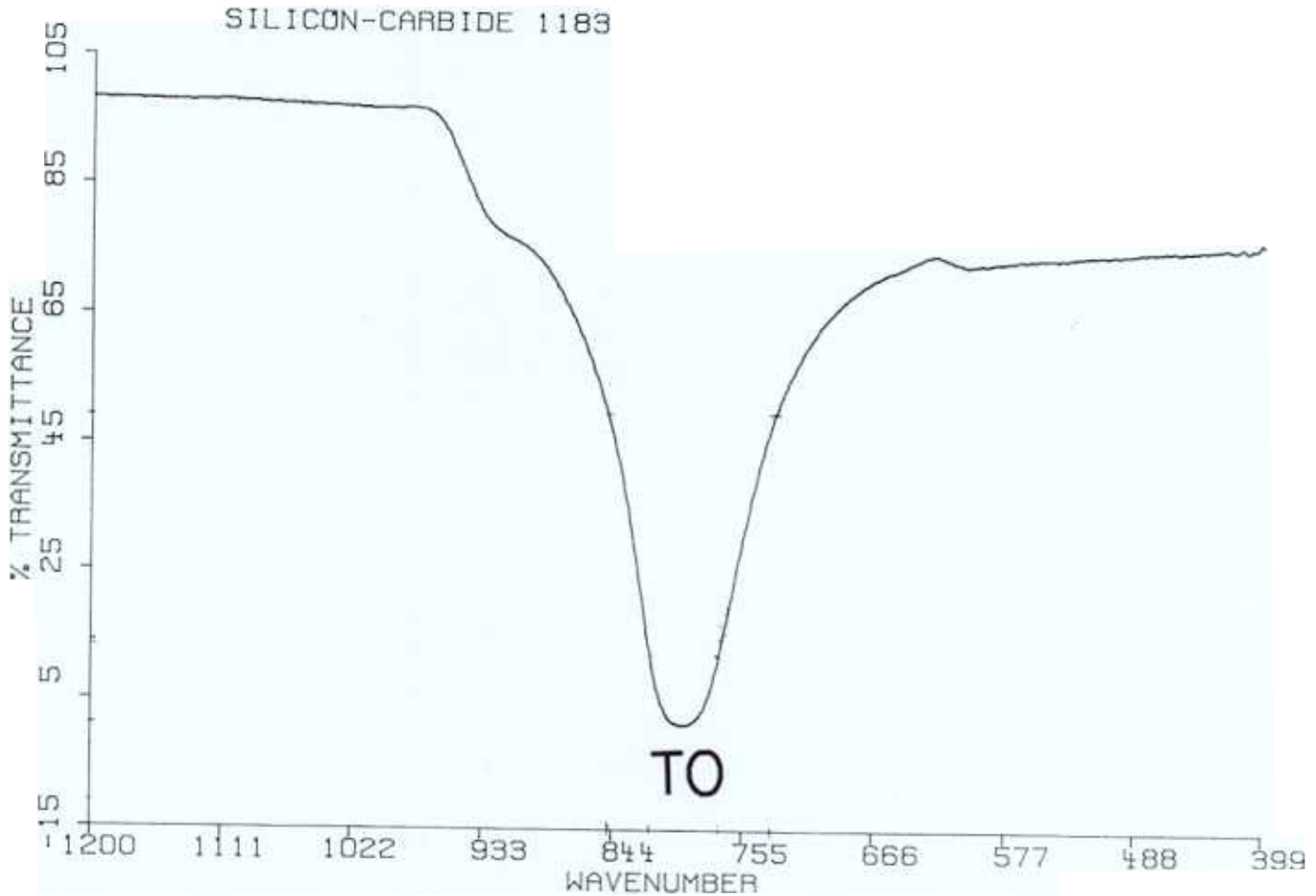


Figure 5.4: The FTIR spectrum of of a $0.3 \mu\text{m}$ 800°C grown film (sample 1183). It showed an absorption peak at 796 cm^{-1} (TO phonon absorption) with a FWHM of 50 cm^{-1} , which is similar to that of the films grown by conventional high temperature growth methods [82].

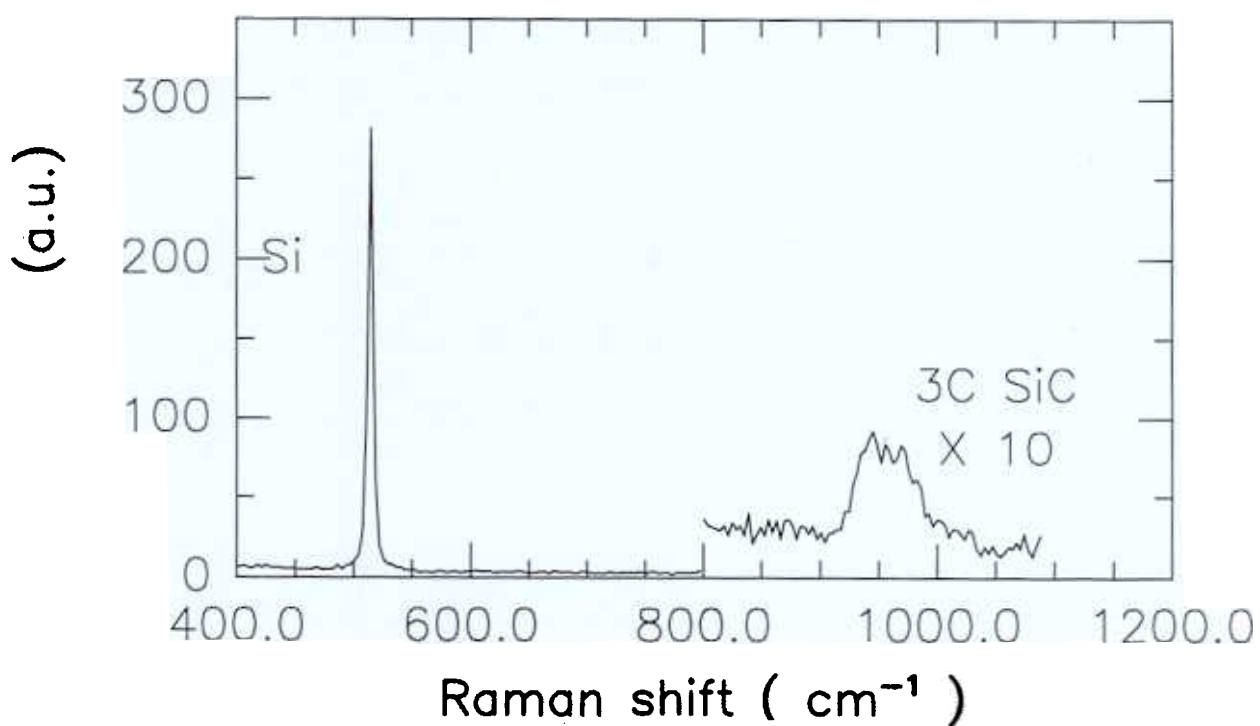


Figure 5.5: The Raman spectrum of of a 0.3 μm 800°C grown film (sample 1183). It showed a broad peak at 960 cm^{-1} with FWHM of 60 cm^{-1} , which is about 10 cm^{-1} below the LO phonon shift ($\sim 970 \text{ cm}^{-1}$) and probably correlated with the interface defects between SiC and Si [83].

single crystalline growth by this technique, in contrast to what is often observed in conventional growth techniques which require high growth temperatures to improve crystallinity.

5.3 Impurity incorporation

Unintentionally doped 3C SiC layers always show n-type conduction [84]. Although there was some controversy initially, there appears to be agreement that the origin of the n-type conduction is controlled by a shallow donor (nitrogen) with binding energy of 15-20 meV [84]. The p-type dopant of Al is popularly used to obtain p-type SiC, because of its relatively low acceptor binding energy of 0.24 eV, compared to boron with the value of 0.735 eV. Another n-type dopant, phosphorus, does not attract enough attention to researchers. Very limited studies of phosphorus-doped SiC have been reported.

Because boron and phosphorus sources (10 ppm B_2H_6 and 70 ppm PH_3 in hydrogen) were already available in our RTCVD reactor, their incorporation into 800 °C 3C SiC growth was measured by SIMS (secondary ion mass spectroscopy, Evans East, Fig. 5.7). Both showed approximately linear incorporation with gas flow up to the concentrations of $5 \times 10^{20} \text{cm}^{-3}$ and $3 \times 10^{20} \text{cm}^{-3}$ for boron and phosphorus, respectively (Fig. 5.8). No systematic Hall measurements or direct electrical activation measurements vs dopant level were performed. The SIMS data (sample 1290) also indicated that there were large amounts of oxygen and hydrogen contamination in our SiC films grown at 800 °C with the concentrations of $3 \times 10^{19} \text{cm}^{-3}$ and $2 \times 10^{19} \text{cm}^{-3}$, respectively. One interesting observation is that phosphorus incorporation reduced the growth of SiC as shown in Fig. 5.1. Boron incorporation will be utilized to compensate the background impurities of the SiC films. This will increase the breakdown voltage of Schottky diodes fabricated on SiC films as shown in next section.

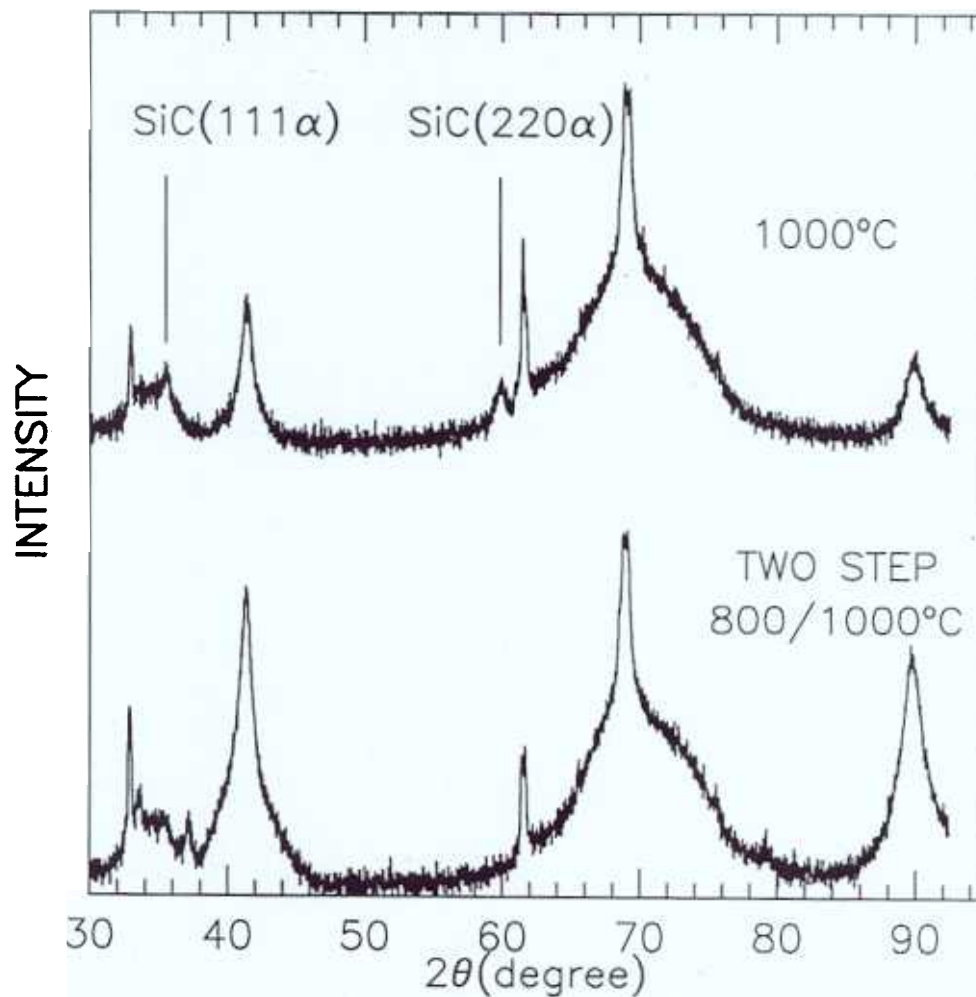


Figure 5.6: The XRD spectra of a 1000°C film (a) and a "two-step" film (b). The film with a thickness of 0.45 μm grown at 1000 °C formed a polycrystalline structure. However, if a 0.15 μm layer was deposited at 800 °C first, then followed by a 0.3 μm film grown at 1000 °C, this led to single crystalline growth at 1000 °C again.

5. Structural and Electrical Studies of Low-Temperature β SiC on Si 81

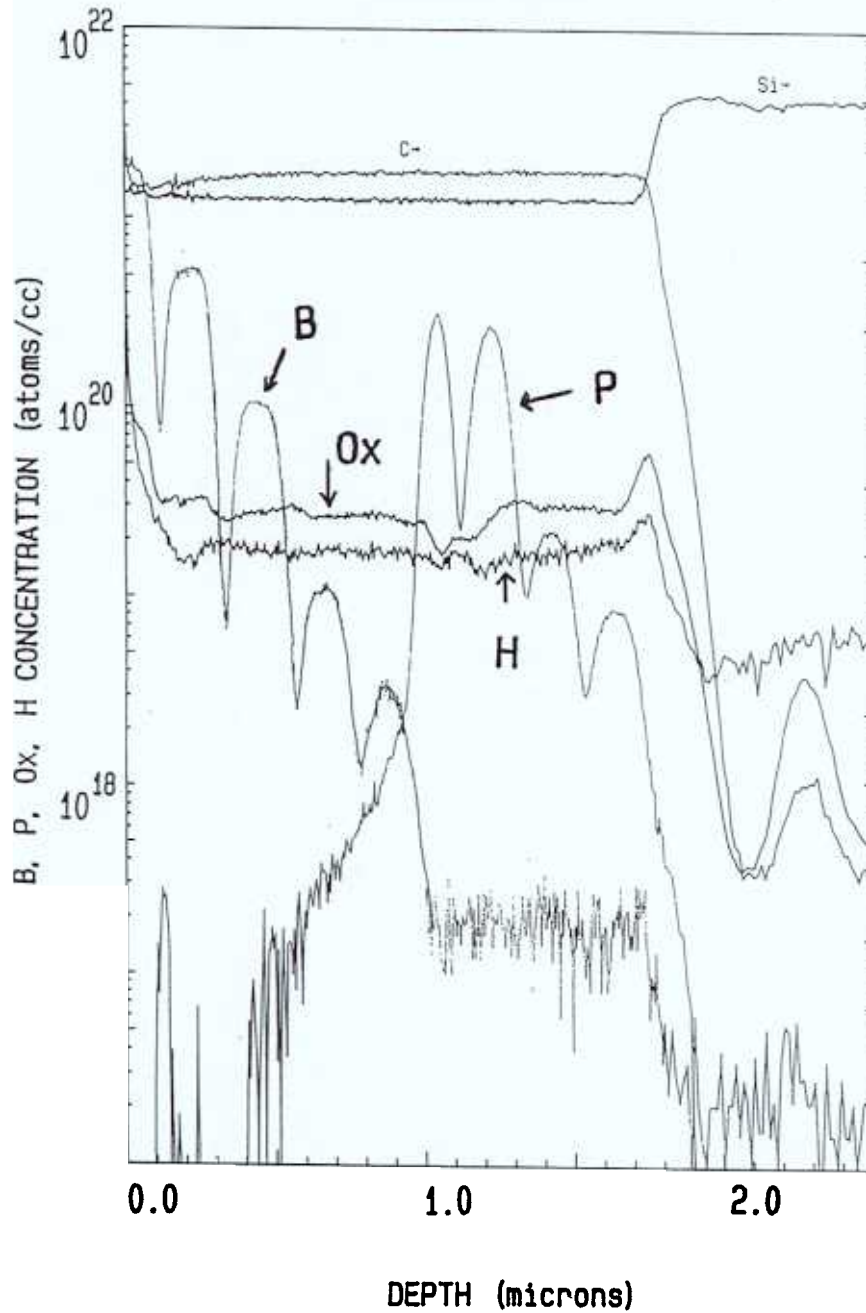


Figure 5.7: SIMS plot of SiC multilayers with impurity incorporations. The growth temperature was 800 °C. The oxygen and hydrogen contamination were $3 \times 10^{19} \text{cm}^{-3}$ and $2 \times 10^{19} \text{cm}^{-3}$, respectively. The bumps are the doped layers with different phosphine (or diborane) flows. The valleys are the undoped spacers.

5. Structural and Electrical Studies of Low-Temperature β SiC on Si 82

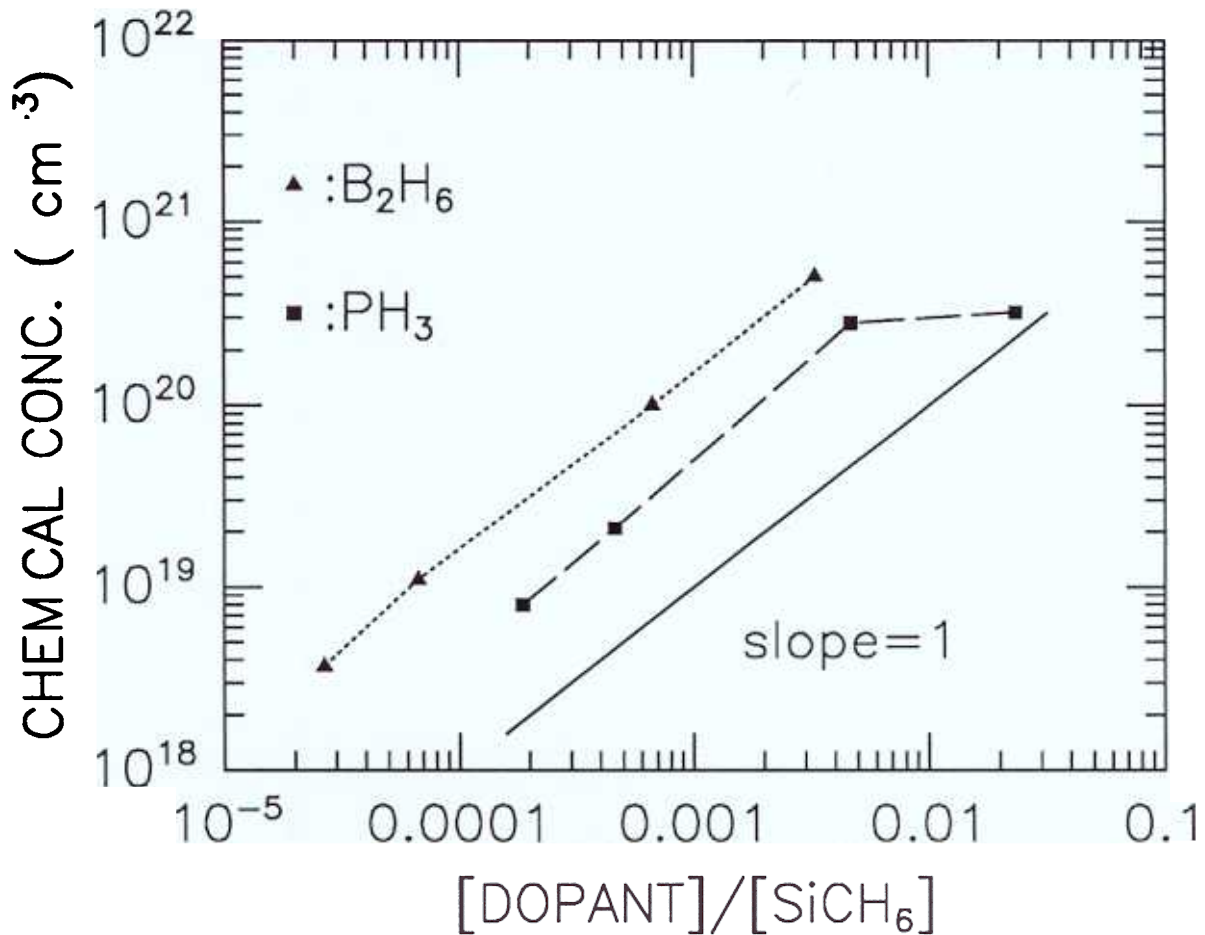


Figure 5.8: The chemical concentrations of dopant (P and B) in SiC as a function of the ratios of actual dopant flow to methylsilane flow. The growth temperature was 800 °C. Both showed linear incorporations up to the concentrations of $5 \times 10^{20} \text{ cm}^{-3}$ and $3 \times 10^{20} \text{ cm}^{-3}$ for boron and phosphorous, respectively. The hydrogen flow was 500 sccm, the methylsilane flow was 1.5 sccm, and the growth pressure was 1 torr.

5.4 Schottky barrier fabrication

All samples used for Schottky barriers were grown at 800°C. Since the unintentionally doped SiC films were n-type with carrier concentrations around 10^{18} cm^{-3} or higher as determined by Hall measurement, boron compensation was necessary to reduce the net dopant concentration of SiC films. The chemical concentration of boron used for this purpose was about 10^{20} cm^{-3} (measured by SIMS in samples grown under similar conditions). However, most boron might be located in nonelectrically active interstitial sites [85]. The electrically active acceptor concentration is estimated about 1 % of the chemical concentration [86]. Therefore, the active acceptor concentration was the same order of magnitude of the background donor concentration. To get the least amount of net dopant concentration in the SiC layers, sometimes we grew a series of films with different B_2H_6 flows, and then picked the best diodes fabricated from those films.

Before metal evaporation, the boron-compensated n-type SiC films were cleaned in dilute HF without any extra polishing, oxidation and etching [80]. The size of Schottky barriers was defined either by photolithography or by shadow masks. Two kinds of Schottky barrier structures were studied:

(a) Al (500nm) Schottky barriers of size $1.3 \times 10^{-4} \text{ cm}^2$ were fabricated on $0.4 \mu\text{m}$, $3 \times 10^{17} \text{ cm}^{-3}$ n-type SiC, with a $2 \mu\text{m}$, $1 \times 10^{16} \text{ cm}^{-3}$ n-type Si buffer on not-tilted Si (100) n-type substrates as shown in the insert of Fig. 5.9 (sample 1221).

(b) Pt (80nm) Schottky barriers of size $1.3 \times 10^{-3} \text{ cm}^2$ were fabricated on $0.4 \mu\text{m}$, $1 \times 10^{16} \text{ cm}^{-3}$ n-type SiC with similar buffers, but on tilted p-type substrates as shown in the insert of Fig. 5.10 (sample 1400).

Because of rough morphology of thick layers ($> 0.5 \mu\text{m}$) grown on not-tilted substrates, the structure (b) was grown on tilted substrates which reduced the leakage current of the Schottky diodes. The Al was deposited by a thermal evaporator. The

Pt evaporation was performed by an electron beam evaporator. Instead of being held at elevated temperature [87], our samples were not intentionally heated during Pt evaporation. The net dopant concentration of SiC were measured by capacitance-voltage measurement after the Schottky barriers were made.

5.5 Results and discussion

The diodes were evaluated using measurement of current-voltage (I-V) and high frequency C-V (capacitance-voltage at 1 MHz) in a light-tight box. One probe made contact to the Schottky barrier itself and the other to a large metal contact away from the barrier. The reverse I-V characteristics of the Al Schottky barriers (type (a)) had a hard breakdown voltage of 13 V (Fig 5.9). To avoid the effect of reverse leakage current, the value of breakdown voltage is obtained by extrapolation of the current at breakdown to the x-axis (voltage axis). The depletion depth at the breakdown was about 0.2 μm (obtained from C-V measurement), and was completely confined in the SiC layer. The breakdown electric field calculated from breakdown voltage and doping concentration was 1×10^6 V/cm, about one third of theoretical value for 3C SiC [88]. The temperature coefficient of breakdown voltage showed a positive value of about 2×10^{-4} $^{\circ}\text{C}^{-1}$ from room temperature to 120 $^{\circ}\text{C}$, and became negative above 190 $^{\circ}\text{C}$ with soft breakdown. Unlike the previous reported negative value[89] for Schottky barriers on 3C SiC heteroepitaxially grown on 6H SiC, this is the first observation of a positive temperature coefficient in 3C or 6H SiC grown by any methods. This also indicates that IMPATT (impact ionization avalanche transit time) diodes can possibly be made in 3C SiC, because the positive temperature coefficient is the direct result of an impact ionization process [90], required for the IMPATT diodes. Combined with the high electron saturation velocity (two times of Si value), the IMPATT diodes based on 3C SiC material might reach an oscillation frequency

5. Structural and Electrical Studies of Low-Temperature β SiC on Si 85

of 200 Ghz. Because the electron energy required for avalanche process is at least 1.5 times bandgap [91] (In Si, the value is 3.6 eV for electrons and 5.0 eV for holes.), the negative temperature coefficient of 6H SiC diodes [92] might be due to the relatively small bandwidth of 6H SiC conduction band and the high bandgap value of 6H SiC (3 eV) such that the electron can not have enough kinetic energy for ionization process. The Al Schottky barriers showed the same I-V characteristics after annealing at 500 °C for 10 min. in forming gas without any degradation.

The reverse I-V characteristics of Pt Schottky barriers in Fig 5.10 showed 60 V breakdown voltage, and the depletion depth at breakdown was 2.5 μm obtained from C-V measurement, implying that the entire SiC layer (1 μm) was depleted and the depletion region terminated in the n-type Si layer. The electric field in SiC and Si, calculated from Poisson's equation, did not reach the breakdown field of either SiC (1×10^6 V/cm) or Si ($\sim 4 \times 10^5$ V/cm). The breakdown probably occurred at the interface defects between SiC and Si, which was suggested by Raman spectroscopy (section 5.2). The temperature coefficient of breakdown voltage had a negative value of 4×10^{-4} °C⁻¹ from room temperature to 120 °C. The Pt Schottky barriers degraded after forming gas annealing at 500 °C for 10 min., showing a soft breakdown around 10 V. This is contrary to the results of Ref. [87], where the Pt Schottky barriers showed improved reverse I-V characteristics at reverse bias of a few volts after isochronal annealing.

The breakdown voltage should be improved by grown n⁺ SiC layer below the active SiC layer to terminate all the electric field lines before the field lines reach the interface.

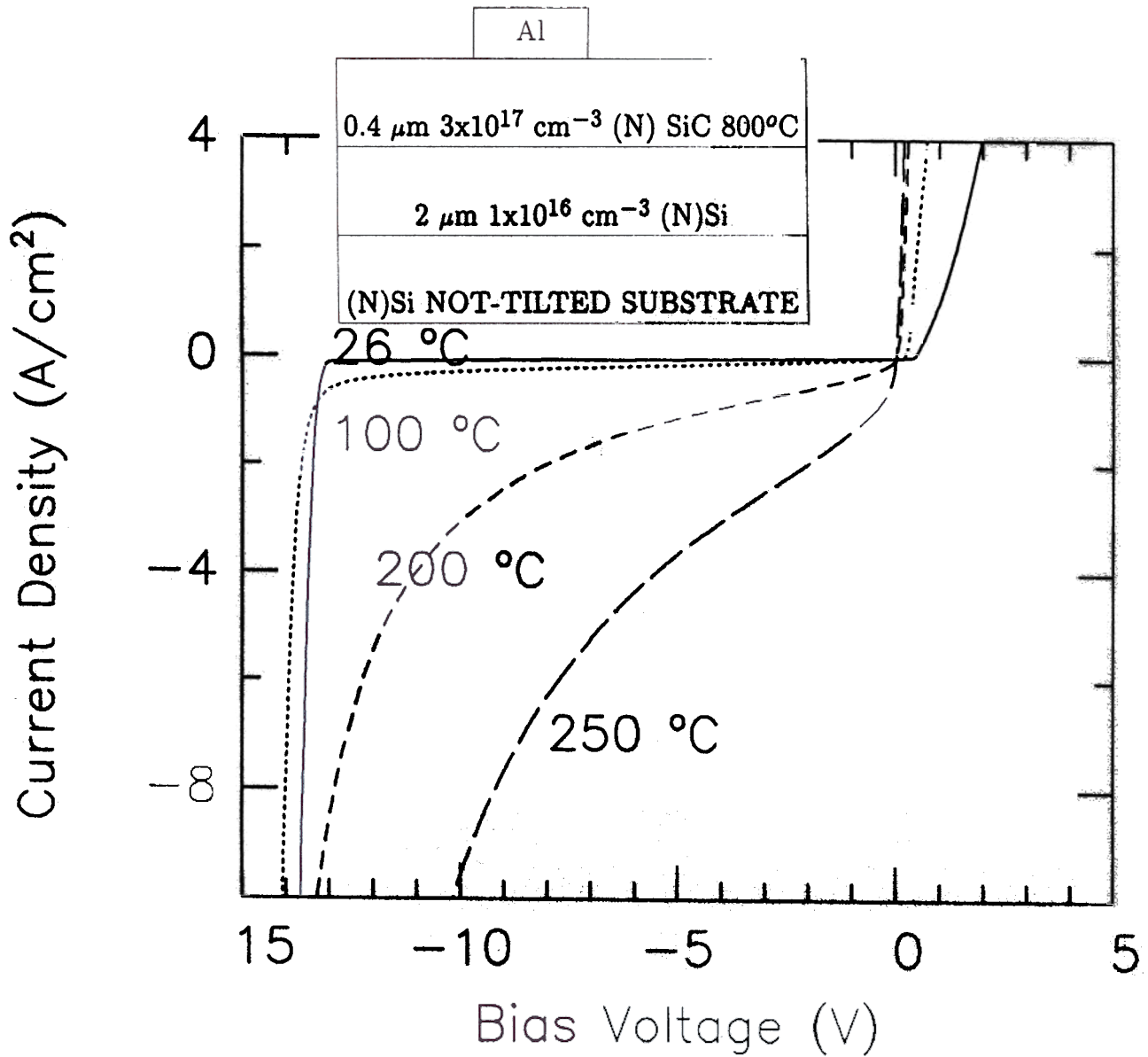


Figure 5.9: The I-V characteristics of Al Schottky barriers. The insert is the device structure. The Al Schottky barriers had a hard breakdown voltage of 13 V with a positive temperature coefficient of about $2 \times 10^{-4} \text{ }^\circ\text{C}^{-1}$ from room temperature to 120 °C, and became negative above 190 °C with soft breakdown.

5. Structural and Electrical Studies of Low-Temperature β SiC on Si 87

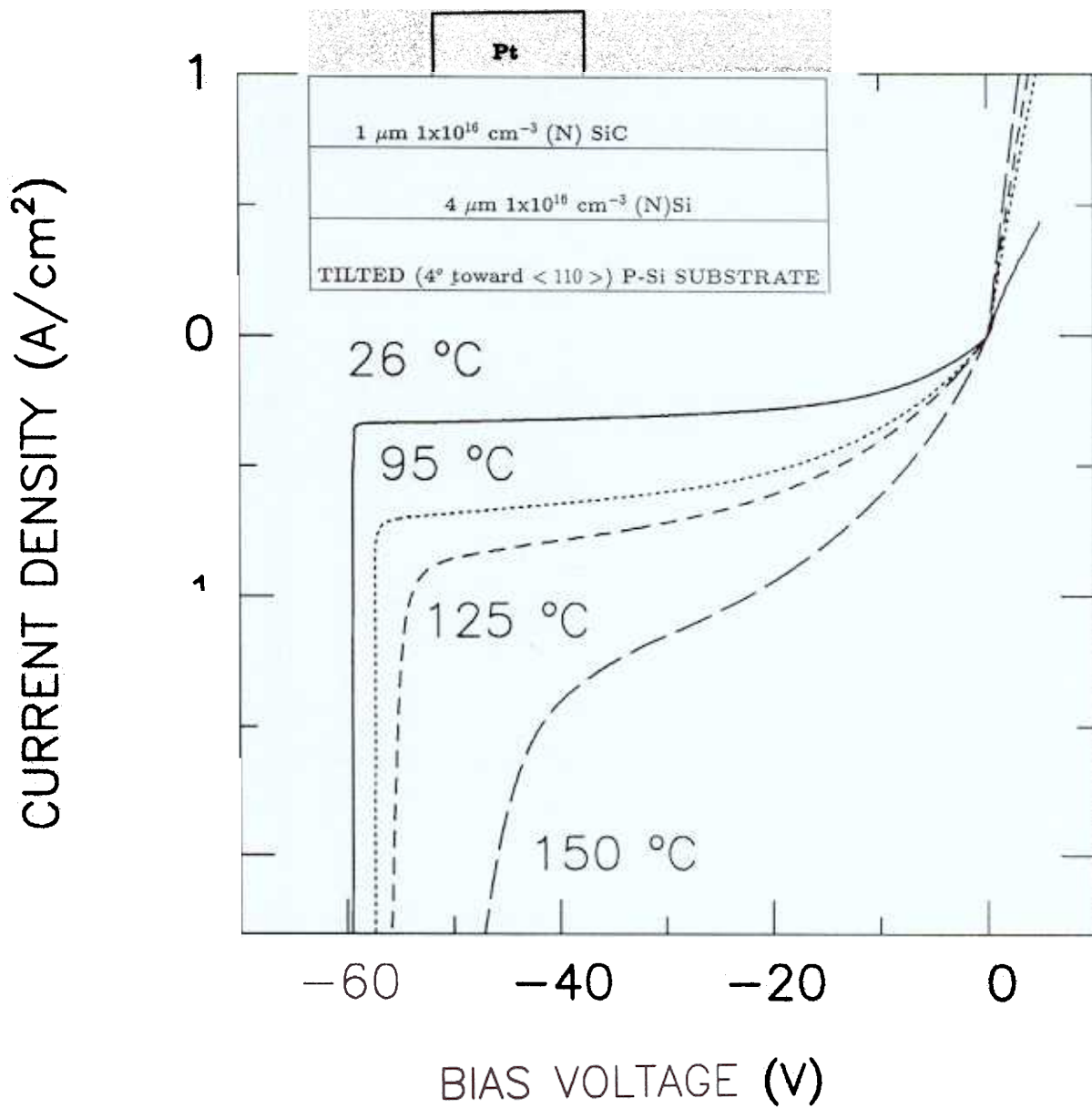


Figure 5.10: The I-V characteristics of Pt Schottky barriers. The insert is the device structure. The Pt Schottky barriers had a hard breakdown voltage of 60 V with a negative temperature coefficient of about $4 \times 10^{-4} \text{ }^\circ\text{C}^{-1}$ from room temperature to 120 $^\circ\text{C}$.

coefficient of breakdown voltage of SiC Schottky diodes may encourage the continuous research interest on 3C SiC IMPATT diodes. We also demonstrates the 60 V breakdown Schottky diodes on the 3C SiC, with possible further increase of the breakdown voltage.

For the novel material of single crystalline SiGeC random alloys, we created the ability to incorporate the C content as high as 1.6 %. The transitions of single crystalline material to amorphous material, then to polycrystalline material were observed for the precursors used in this study.

7.2 Future work

From a material point of view, two kinds of technologies will be very useful for the Si-based electronic and optoelectronic devices. They are Ge epitaxy and wide bandgap materials for Si HBTs.

The precise control of Ge growth in the monolayer scale is necessary to fabricate the zone-folding structures [103] to possibly increase the matrix elements of optical transition in Si/Ge material. The Si/Ge superlattices can also hopefully reduce the alloy scattering, which occurs in SiGe random alloy for hole transport, and possibly yields super-high mobility of holes, which is relatively low in SiGe channel of modulation doped structures. However, the Ge growth at 625°C in our RTCVD reactor suffered a intermixing of Si and Ge on the order of 10 Å. Further reduction of the intermixing is required for the applications of Ge growth.

Despite the great success of narrow base Si/SiGe HBTs, the Si/SiGe process is not compatible with existing polysilicon-emitter technologies [1, 93]. Therefore, it will be difficult to produce on a VLSI scale. A wide bandgap emitter may be necessary to push Si HBT technology into VLSI circuits. One obvious candidate is β SiC with the bandgap of 2.2 eV [94]. However, our initial study of β SiC/Si HBTs showed

lector currents for both devices showed same voltage (V_{be}) dependence with ideality factor of 1. This result is expected, because both devices have the same base structures. The base currents also showed near-ideal behavior with ideality factors of 1.1 and 1.2 for Si BJT and SiC/Si HBT, respectively. However, the desired enhancement of current gain (I_c/I_b) was not observed, because the base current of SiC/Si HBT was higher than that of Si BJT. The increase of base current in the SiC/Si HBT, compared to the Si BJT, was probably due to the interface defects between Si and SiC, which acted as recombination centers for back-injected holes and thus increased the hole current, instead of being the barrier to stop the hole current.

To reduce the defect density at the interface and to increase the current gain, a passivation technology of the interface will be desired in the future.

5.7 Summary

Device quality 3C SiC has been grown at 800 °C on Si for the first time. The growth temperature of 800 °C was essential for initial single crystalline SiC growth on Si (100) substrates and a "two step" growth technique was developed to improve the crystalline quality of the films grown at high temperature. Schottky barriers on n-type SiC on (100) Si showed a reverse breakdown voltage as high as 60 V. A positive temperature coefficient of breakdown voltage of 3C SiC was observed for the first time.

Si BJT (sample 1200)

$n^+(10^{18}\text{cm}^{-3})$	– Si emitter	$\sim 2000 \text{ \AA}$	(800 °C)
$n(10^{17}\text{cm}^{-3})$	– Si emitter	$\sim 3000 \text{ \AA}$	(800 °C)
$p^+(10^{19}\text{cm}^{-3})$	– Si base	$\sim 600 \text{ \AA}$	(700°C)
$n(10^{17}\text{cm}^{-3})$	– Si collector	$\sim 3000 \text{ \AA}$	(800°C)
$n^+(10^{19}\text{cm}^{-3})$	– Si collector	$\sim 2\mu\text{m}$	(1000°C)

< 100 > not-tilted n Si substrates

SiC/ Si HBT (sample 1201)

$n^+(10^{18}\text{cm}^{-3})$	– Si emitter	$\sim 2000 \text{ \AA}$	(800 °C)
$n^+(10^{18}\text{cm}^{-3})$	– SiC emitter	$\sim 2000 \text{ \AA}$	(800 °C)
$n(10^{17}\text{cm}^{-3})$	– Si emitter	$\sim 3000 \text{ \AA}$	(800 °C)
$p^+(10^{19}\text{cm}^{-3})$	– Si base	$\sim 600 \text{ \AA}$	(700°C)
$n(10^{17}\text{cm}^{-3})$	– Si collector	$\sim 3000 \text{ \AA}$	(800°C)
$n^+(10^{19}\text{cm}^{-3})$	– Si collector	$\sim 2\mu\text{m}$	(1000°C)

< 100 > not-tilted n Si substrates

Figure 5.11: Layer structures of Si bipolar junction transistors and SiC/Si heterojunction bipolar transistors. There is an additional SiC layer between the n-Si emitter and the n^+ -Si emitter in the SiC/Si HBT.

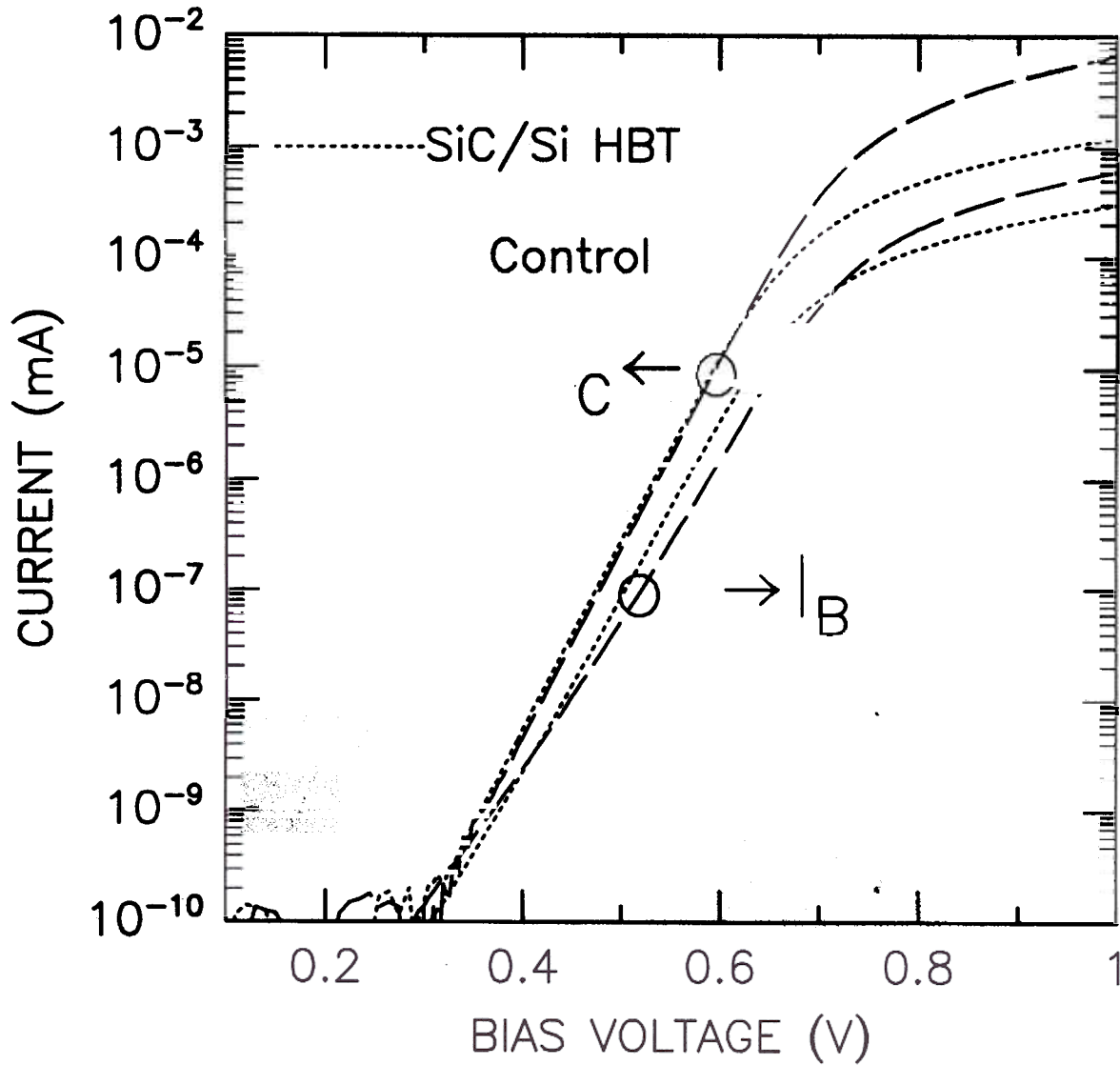


Figure 5.12: The Gummel plots of SiC/Si HBT and Si control device. The base currents of β SiC/Si HBT were higher than those of Si control bipolar transistors, while the collector currents for both devices were very similar (they had identical base structures).

Single Crystalline SiGeC random alloys

6.1 Introduction

Due to the wide bandgap (5 eV) of diamond, the substitutional incorporation of carbon into SiGe may provide a material complementary to SiGe for bandgap engineering of Si-based heterojunctions [96]. Furthermore, the small lattice constant (50% smaller than Si) of diamond can also provide tensile strain in the SiGeC grown on Si to compensate the compressive strain induced by the large Ge atoms. Regoloni *et al.* [97] have shown that the addition of 0.6% C into $\text{Si}_{0.8}\text{Ge}_{0.2}$ layers on Si substrates can increase the epitaxial layer thickness up to 390 nm at the growth temperature of 625 °C without any dislocation generation, compared to the metastable equilibrium critical thickness of 150 nm for $\text{Si}_{0.8}\text{Ge}_{0.2}$ (section 2.2). The “strain compensation” introduces an additional design parameter in SiGe (C) material growth. If Vegard’s law applies to the SiGeC system, one expects that 10.8% Ge can be compensated by 1% C in the pseudomorphic SiGeC film.

The main challenge in fabricating such alloys is to minimize the thermodynamically favorable tendency to form silicon carbide phase instead of obtaining C atoms in substitutional sites. Several techniques have been reported for fabricating SiGeC alloys. Ebert *et al.* [98] used MBE to grow SiGeC at the temperature of 400–550°C with graphite as a carbon source. Im *et al.* [99] used Solid Phase Epitaxy to obtain

SiGeC alloys by implantation of C and Ge into Si, followed by solid phase regrowth at 800 °C. However, no electrical or optical results have been obtained from the alloys grown by these two techniques.

Recently, Boucaud *et al.* [100] reported photoluminescence measurements of a SiGeC alloy grown by RTCVD at 550 °C with C concentration up to 0.8 %. However, there were deep level transitions in the photoluminescence spectra, indicating some imperfect crystallinity in their SiGeC films.

In this chapter, the growth of SiGeC by RTCVD at 550 °C using methylsilane as a carbon source with germane and dichlorosilane/silane mixture is reported. The C concentration as high as as 1.6 % is obtained.

6.2 Growth and characterization

The ternary alloys SiGeC were deposited on Si (100) substrates at 550 °C at a growth pressure of 6 torr by RTCVD with either silane or dichlorosilane as Si sources. For DCS growth, the gas flows were 3 slpm for a hydrogen carrier, 26 sccm for DCS, and 100 sccm for the germane mixture flow (0.8 % in hydrogen), and the methylsilane vapor flow varied from 0.8 to 12 sccm. For silane growth, DCS was replaced by silane with 250 sccm flow (4 % in hydrogen), the methylsilane flow was 0.1 to 0.8 sccm, and the other flows were maintained at the same conditions. The growth rates obtained from sputter Auger profiling were about 4 Å/min. and 16 Å/min. for DCS and silane growth, respectively (for zero methylsilane flow), and the small amount of methylsilane addition was assumed to have little effect on growth rates. The crystallinity of the SiGeC alloys was studied by Double Crystal X-ray Diffraction (DCXRD), Fourier Transform Infrared Spectroscopy (FTIR) and Rutherford back scattering spectroscopy (RBS). For the DCS growth, a series of layers with the same thickness (40 nm) were grown with the methylsilane flows of 0 (sample 1614), 0.8

(sample 1600), 0.15 (also sample 1600), 0.25 (sample 1612), and 0.5 sccm (sample 1601). No dislocation lines were observed in any of these films by defect etching (section 2.5.2). The double crystal X-ray rocking curves for these growth conditions are shown in Fig. 6.1

The film without any methylsilane addition revealed a Ge content of 0.25, estimated by Vegard's law with the following formula,

$$x = \Delta\theta/10440 \quad (6.1)$$

where x is the Ge content, $\Delta\theta$ is the separation of (400) peaks between the SiGe layer and the Si substrate in the unit of arc second. The addition of methylsilane led to the shift of SiGeC (400) peaks towards the Si (400) peak up to a methylsilane flow of 0.25 sccm (Fig. 6.1(c)). This indicates the strain in the SiGeC alloy was reduced. Note that the broad peaks of all SiGeC alloys were due to the small thickness of those films. Assuming that the Ge content is the same with the addition of the small amount of methylsilane and using the compensation ratio of 1 % C to 10.8 % Ge obtained from Vegard's law, we can also estimate the C concentration of these layers. The maximum C concentration was 1.6% for the methylsilane flow of 0.25 sccm. Further increase of methylsilane flow to 0.5 sccm yielded layers with no crystalline peaks (amorphous layers) observed in the rocking curve, Fig. 6.1(d)).

To study the structure of the SiGeC alloys with higher flows of methylsilane, the FTIR measurements were performed. Three distinct types of FTIR spectra (Fig. 6.2) were observed for DCS growth, depending on the methylsilane flow. At low flow (0.25 sccm, sample 1592), the FTIR showed a sharp vibration at 600 cm^{-1} , which is characteristic of the vibration frequency of substitutional C in Si [101], consistent with the DCXRD results in Fig.6.1, indicating a crystalline layer. At intermediate flow (1.5 sccm, sample 1591), a broad peak from 600 cm^{-1} to 840 cm^{-1} was observed, very similar to the absorption spectrum of amorphous silicon carbide [102]. This is

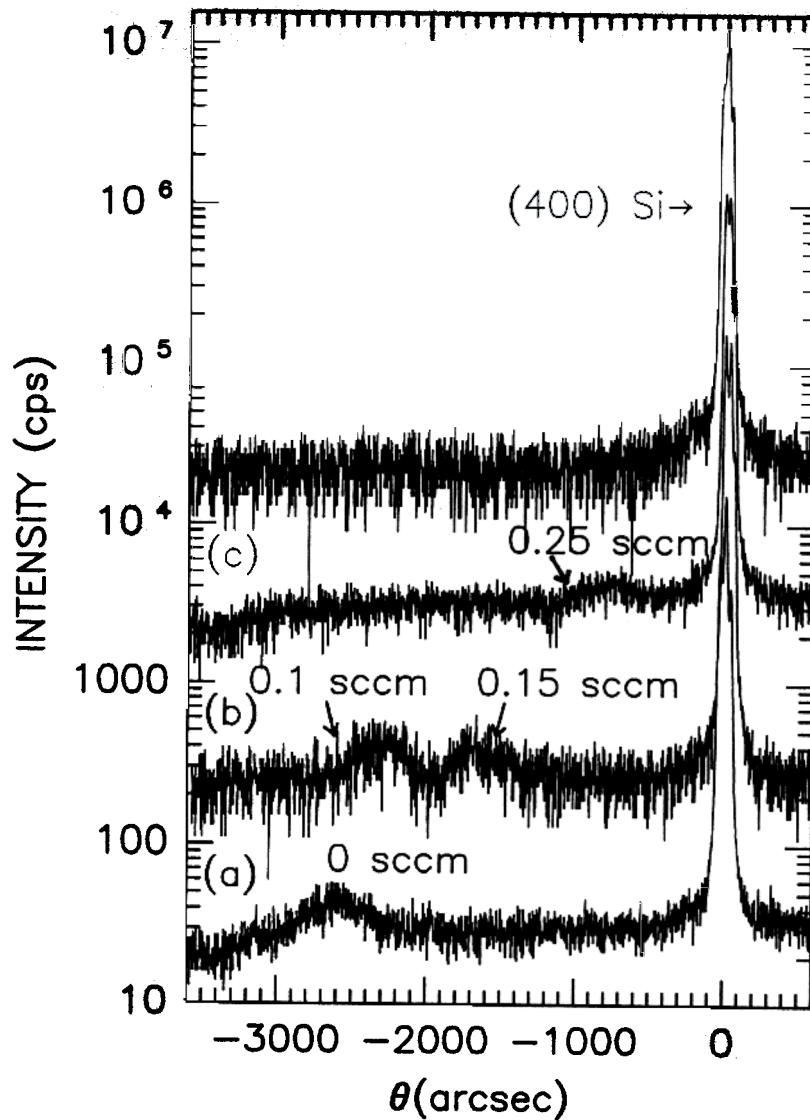


Figure 6.1: The double crystal X-ray rocking curves of SiGeC alloy layers grown by DCS. The addition of methylsilane led to the shift of SiGeC (400) peaks towards the Si (400) peak up to a methylsilane flow of 0.25 sccm. This indicates the strain in the SiGeC alloy was reduced. Further increase of methylsilane flow to 0.5 sccm yielded amorphous layers. Note that sample (b) had two layers of SiGeC alloys.

again consistent with DCXRD results. At high flow (12 sccm, sample 1584), there were two silicon-carbide like absorption peaks around 800 cm^{-1} and 960 cm^{-1} for the vibrations of TO phonon and LO phonon, respectively, indicating the polycrystalline SiC precipitates.

On the other hand, for silane growth, the control SiGe had a Ge content of 22% , again determined by the double crystal rocking curve (Fig. 6.3(a), sample 1597). With an additional methylsilane 0.1 sccm flow, the (400) SiGeC alloy peak shifted a little bit to the Si peak, corresponding to a C concentration of 0.1 % (Fig. 6.3(b), sample 1593). Further increase of the methylsilane flow to 0.2 sccm yielded amorphous growth (Fig. 6.3(c), sample 1598). The FTIR spectrum of the SiGeC alloy with 0.1 sccm (sample 1593) methylsilane flow also showed the 600 cm^{-1} vibration of substitutional C in Si. The alloys with 0.5 (sample 1594) and 0.8 sccm (sample 1586) methylsilane flows had broad peaks similar to those of the DCS grown films, which resembled amorphous SiC. The nominal thickness of the silane grown films were 80 nm.

6.3 Summary

We have successfully fabricated single crystalline SiGeC alloys with C content up to 1.6 % by RTCVD using methylsilane as a C precursor with DCS and germane mixtures. The DCS growth is more favorable than silane growth in terms of C incorporation. As methylsilane flow increases, the transitions of single crystalline SiGeC to amorphous SiC, then to polycrystalline SiC have been observed.

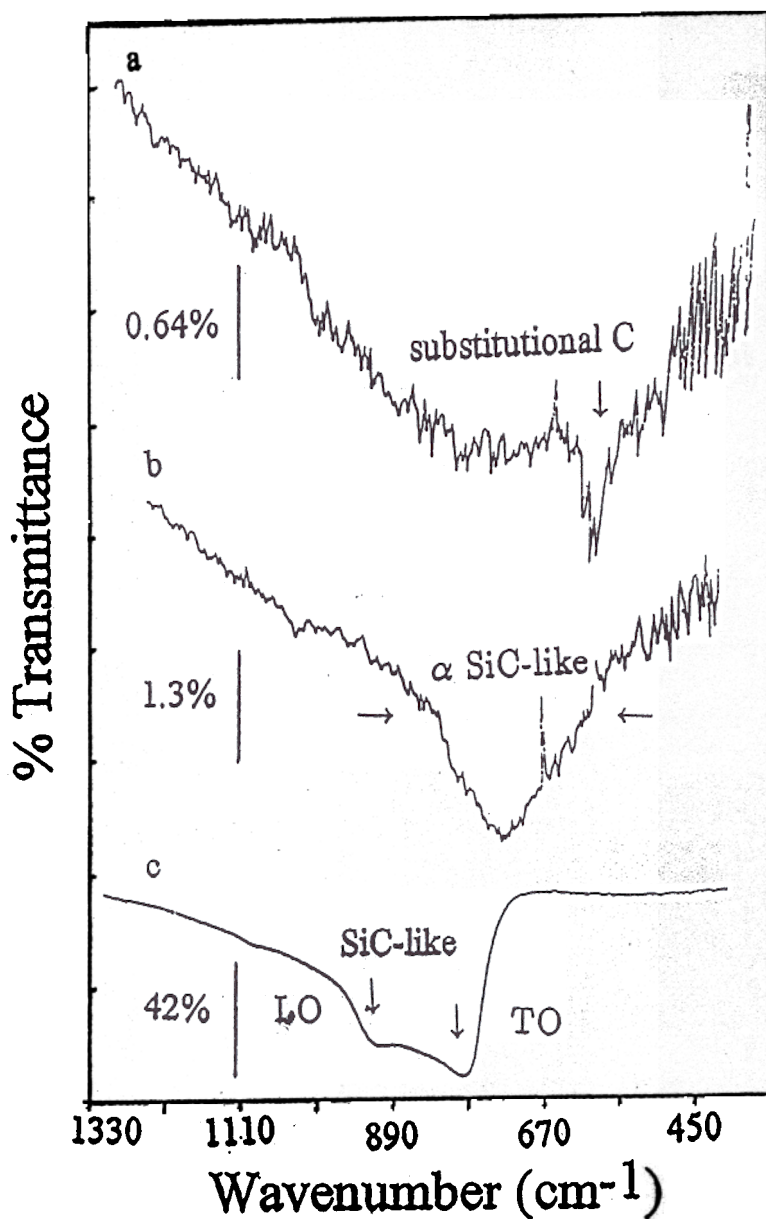


Figure 6.2: FTIR spectra of SiGeC samples grown with DCS at 550 °C. At low flow (0.25 sccm), the FTIR showed a sharp vibration at 600 cm⁻¹, which is characteristic of the vibration frequency of substitutional C in Si. At intermediate flow (1.5 sccm), a broad peak from 600 cm⁻¹ to 840 cm⁻¹ was observed, very similar to the absorption spectrum of amorphous silicon carbide. At high flow (12 sccm), there were two silicon-carbide like absorption peaks around 800 cm⁻¹ and 960 cm⁻¹ for the vibrations of TO phonon and LO phonon, respectively. Note that the scales are different for each spectrum (see the 0.64 %, 1.3 % and 42 % markers).

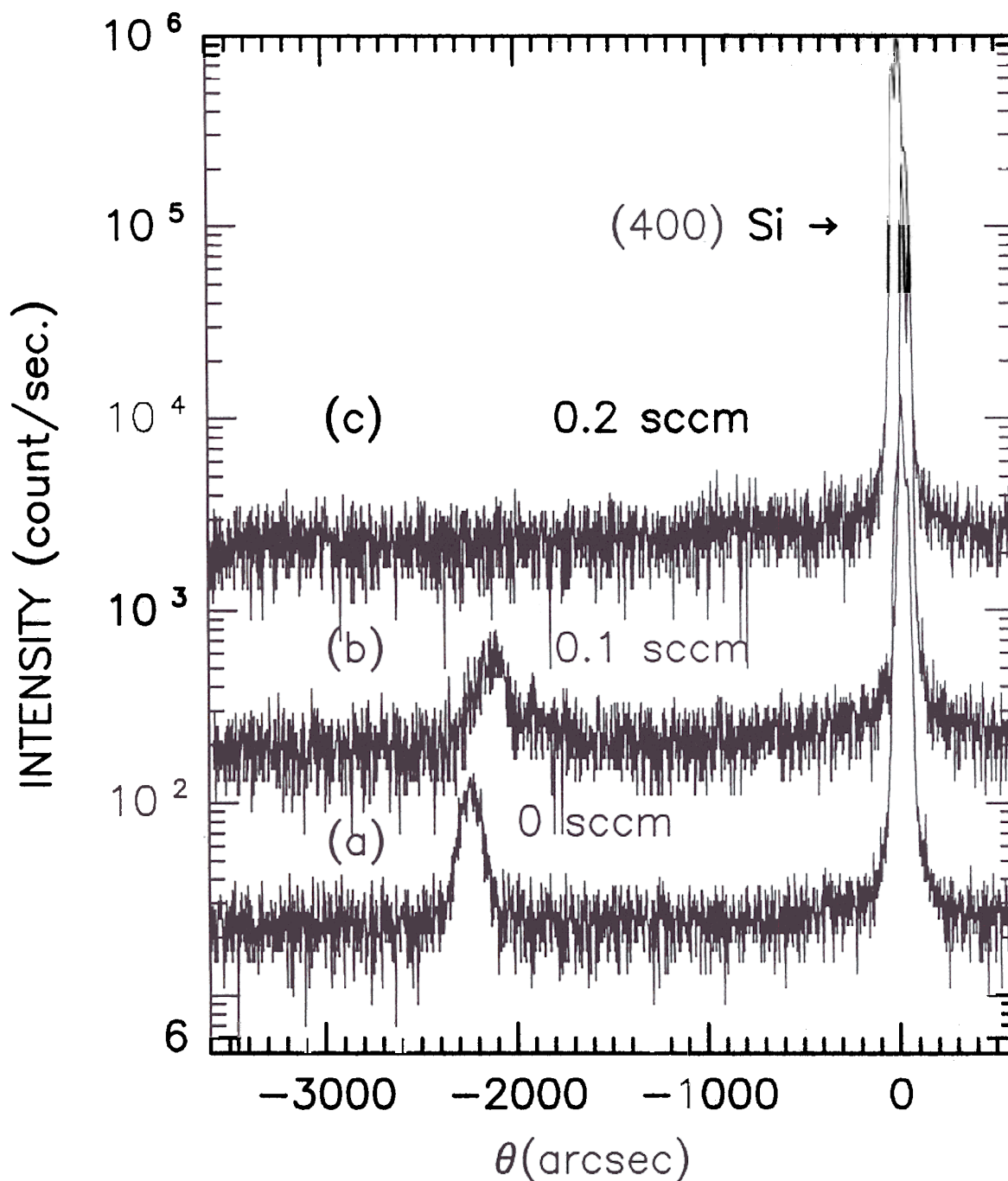


Figure 6.3: The double crystal X-ray rocking curves of SiGeC alloy layers grown by silane. The pure SiGe sample had a Ge content of 22 %. With an additional methylsilane 0.1 sccm flow, the (400) SiGeC alloy peak shifted a little bit to the Si peak, corresponding to a C concentration of 0.1 % . Further increase of the methylsilane flow to 0.2 sccm yielded amorphous growth.

Summary and Future Work

7.1 Summary

The research described in this thesis has concentrated on novel heteroepitaxial growth of column IV material on Si substrates. This includes SiGe, silicon carbide, and SiGeC alloys.

For SiGe, the selective area growth has been demonstrated to reduce the misfit dislocation density. The graded relaxed buffer and strained layer superlattices were used to reduce the threading dislocation density, and novel electronic structures such as electron modulation doped structures and electron resonant tunneling diodes were successfully fabricated on the graded relaxed buffers. The strong light emission of non-phonon process of (110) strained SiGe on Si may lead to the improvement of Si-based light emitting devices. We also measured the bandgap of strained (110) SiGe, which provides a fundamental material parameters for future device design. Furthermore, a new method of measuring the conduction band offset was demonstrated, and the conduction band offsets in strained SiGe on (110) and (100) Si were measured for the first time.

For β SiC, the low temperature growth makes possible the integration of SiC devices on Si substrates. The 800 °C was found essential for single crystalline SiC growth on Si by using the methylsilane. The first observation of positive temperature

coefficient of breakdown voltage of SiC Schottky diodes may encourage the continuous research interest on 3C SiC IMPATT diodes. We also demonstrates the 60 V breakdown Schottky diodes on the 3C SiC, with possible further increase of the breakdown voltage.

For the novel material of single crystalline SiGeC random alloys, we created the ability to incorporate the C content as high as 1.6 %. The transitions of single crystalline material to amorphous material, then to polycrystalline material were observed for the precursors used in this study.

7.2 Future work

From a material point of view, two kinds of technologies will be very useful for the Si-based electronic and optoelectronic devices. They are Ge epitaxy and wide bandgap materials for Si HBTs.

The precise control of Ge growth in the monolayer scale is necessary to fabricate the zone-folding structures [103] to possibly increase the matrix elements of optical transition in Si/Ge material. The Si/Ge superlattices can also hopefully reduce the alloy scattering, which occurs in SiGe random alloy for hole transport, and possibly yields super-high mobility of holes, which is relatively low in SiGe channel of modulation doped structures. However, the Ge growth at 625°C in our RTCVD reactor suffered a intermixing of Si and Ge on the order of 10 Å. Further reduction of the intermixing is required for the applications of Ge growth.

Despite the great success of narrow base Si/SiGe HBTs, the Si/SiGe process is not compatible with existing polysilicon-emitter technologies [1, 93]. Therefore, it will be difficult to produce on a VLSI scale. A wide bandgap emitter may be necessary to push Si HBT technology into VLSI circuits. One obvious candidate is β SiC with the bandgap of 2.2 eV [94]. However, our initial study of β SiC/Si HBTs showed

that the base currents of β SiC/Si HBTs were higher than those of Si control devices. There was no enhancement of current gain in the SiC/Si HBTs with respect to the Si control device. Therefore, future work on SiC/Si structures, possibly including passivated polycrystalline SiC growth at low temperature, is an important direction for future SiC/Si HBTs.

References

- [1] S. Sze, *High-Speed Semiconductor Devices*. John Wiley, New York, N. Y., 1990.
- [2] D. L. Harame and et al., "Optimization of SiGe HBT technology for high speed analog and mixed-signal applications," *IEDM, Tech. Dig.* , p. 71, 93.
- [3] E. Crabbé, B. Meyerson, J. Stock, and D. Harame, "Vertical profile optimization of very high frequency epitaxial Si- and SiGe-base bipolar transistors," *IEDM, Tech. Dig.* , p. 83, 1993.
- [4] E. Kasper, A. Gruhle, and H. Kibbel, "High speed SiGe-HBT with very low base sheet resistivity Si- and SiGe-Base bipolar transistors," *IEDM, Tech. Dig.* , p. 79, 1993.
- [5] D. L. Harame and et al., "30 GHz polysilicon-emitter and single-crystal-emitter graded SiGe-base pnp transistors," *IEDM, Tech. Dig.* , p. 33, 90.
- [6] K. Ismail, B. Meyerson, S. Rishton, J. Chu, S. Nelson, and J. Nocera, "High-transconductance n-type Si/SiGe modulation doped field effect transistors," *IEEE Electron Device Lett.*, vol. 13, p. 229, 1992.
- [7] E. Murakami, K. Nakagawa, A. Nishida, and M. Miyao, "Strained-controlled Si-Ge Modulation-Doped FET with ultrahigh hole mobility," *IEEE Electron Device Lett.*, vol. 12, p. 71, 1991
- [8] K. Ismail, B. Meyerson, and P. Wang, "High electron mobility in modulation-doped Si/SiGe," *Appl. Phys. Lett.*, vol. 58, p. 2117, 1991.

- [9] Z. Matutinovic-Krstelj, C. Liu, X. Xiao, and J. Sturm, "Symmetric Si/SiGe electron resonant tunneling diodes with an anomalous temperature behavior," *Appl. Phys. Lett.*, vol. 62, p. 603, 1993.
- [10] S. Rheed, J. Park, R. Karunasiri, Q. Ye, and K. Wang, "Resonant tunneling through a Si/SiGe/Si heterostructures on a GeSi buffer layers," *Appl. Phys. Lett.*, vol. 53, p. 204, 1988.
- [11] X. Xiao, J. Sturm, S. Parihar, S. Lyon, D. Meyerhofer, and S. Palfrey, "Silicide/SiGe Schottky-Barrier long-wavelength infrared detectors," *IEDM, Tech. Dig.*, p. 125, 92.
- [12] Q. Mi, X. Xiao, J. Sturm, L. Lenchyshyn, and M. Thewalt, "Room-temperature 1.3 μm electroluminescence from strained SiGe/Si quantum wells," *Appl. Phys.* vol. 60, p. 3177, 1992.
- [13] F. Schäffler D. Többen H-J Herzog G. Abstreiter and B. Holländer, "High-electron-mobility Si/SiGe heterostructures: influence of the relaxed SiGe buffer layer," *Semicond. Sci. Technol.*, vol. 7, p. 260, 1992.
- [14] Y. H. Xie, D. Monroe, E. A. Fitzgerald, P. J. Silverman, F. A. Thiel, and G. P. Waston, "Very high mobility two dimension hole gas in Si/Si_{1-x}Ge_x/Ge structures grown by molecular beam epitaxy," *Appl. Phys. Lett.*, vol. 63, p. 2263, 1993.
- [15] J.-P. Cheng, V. Kesan, D. Grutzmacher, T. Sedgwick, and J. Ott, "Cyclotron resonance studies of two-dimensional holes in strained Si_{1-x}Ge_x/Si quantum wells," *Appl. Phys. Lett.*, vol. 62, p. 1522, 1993.
-

- [16] X. Xiao, C. Liu, J. Sturm, L. Lenchyshyn, and M. Thewalt, "Photoluminescence from electron-hole plasmas confined in Si/Si_{1-x}Ge_x/Si quantum wells," *Appl. Phys. Lett.*, vol. 60, p. 1720, 1992.
- [17] E. A. Fitzgerald, P. D. Kirchner, R. Proano, G. D. Pettit, J. M. Woodall, and D. G. Ast, "Elimination of interface defects in mismatched epilayers by a reduction in growth area.," *Appl. Phys. Lett.*, vol. 52, p. 1496, 1988.
- [18] J. C. Bean, "Strained layer epitaxy of germanium silicon alloys," *Science*, vol. 230, p. 127, 1985.
- [19] D. Hull and D. J. Bacon, *Introduction to dislocations*. 3rd ed. Pergamon Press, Oxford, 1984. Chap. 4.
- [20] K. Kamigaki, F. Sakashita, H. Kato, M. Nakayama, N. Sano, and H. Terauchi, "X-ray study of misfit strain relaxation in lattice-mismatched heterojunctions," *Appl. Phys. Lett.*, vol. 49, p. 1017, 1986.
- [21] J. W. Matthews, *Epitaxial growth*. Academic Press, New York, 1975. Chap. 8, p. 562.
- [22] T. Pearsall, ed., *Semiconductor and Semimetals, Vol. 32, Strained-Layer Superlattice: Physics*. Academic, New York, NY, 1990. p.24.
- [23] M. Neuberger, *Hand book of electronic materials volume 5: Group IV semiconducting materials*. IFI/PLENUM, New York, 1971. p 37.
- [24] D. C. Houghton, C. J. Gibbings, C. G. Tuppen, M. H. Lyons, and A. G. Halliwell, "Equilibrium critical thickness for Si_{1-x}Ge_x strained layers on (100) Si," *Appl. Phys. Lett.*, vol. 56, p. 460, 1990.
-

- [25] R. People and J. C. Bean, "Erratum: Calculation of critical thickness versus lattice mismatch for $\text{Si}_{1-x}\text{Ge}_x/\text{Si}$ strained layer heterostructure," *Appl. Phys. Lett.*, vol. 49, p. 229, 1986.
- [26] P. M. Maree, J. C. Barbour, J. F. van der Veen, K. L. Kavanagh, C. W. T. Bulle-Lieuwma, and M. P. A. Vieggers, "Generation of misfit dislocation in semiconductors," *Appl. Phys. Lett.*, vol. 62, p. 4413, 1987.
- R. People, "Indirect bandgap of coherently strained $\text{Si}_{1-x}\text{Ge}_x$ bulk alloy on (001) silicon substrates," *Phys. Rev. B*, vol. 32, p. 1405, 1985.
- [28] X. Xiao, *Silicon-germanium alloys for optoelectronic applications*. PhD thesis, Princeton University, 1993.
- [29] C. van de Walle and R. Martin, "Theoretical calculations of heterojunction discontinuities in the Si/Ge system," *Phys. Rev. B*, vol. 34, pp. 5621–5634, 1986.
- J. Sturm, P. Schwartz, E. Prinz, and H. Manoharan, "Growth of $\text{Si}_{1-x}\text{Ge}_x$ by rapid thermal chemical vapor deposition and application to heterojunction bipolar transistors," *J. Vac. Sci. Technol. B*, vol. 9, p. 2011, 1991.
- P. Schwartz and J. Sturm, "Microsecond carrier lifetimes in strained silicon-germanium alloys grown by rapid thermal chemical vapor deposition," *Appl. Phys. Lett.*, vol. 57, p. 2004, 1990.
- [32] J. Sturm, P. Garone, and P. Schwartz, "Temperature control of silicon-germanium alloy epitaxy growth on silicon substrate by infrared transmission," *J. Appl. Phys.*, vol. 69, p. 542, 1990.
-

- [33] J. Sturm and E. Prinz, "Graded base Si/Si_{1-x}Ge_x/Si heterojunction bipolar transistors grown by rapid thermal chemical vapor deposition with near-ideal electrical characteristics," *IEEE Electron Device Lett.*, vol. 12, p. 303, 1991
- [34] E. Prinz and J. Sturm, "Current gain-Early voltage products in heterojunction bipolar transistors with nonuniform base bandgaps," *IEEE Electron Device Lett.*, vol. 12, p. 661, 1991
- [35] J. Sturm, H. Manoharan, L. Lenchyshyn, M. Thewalt, N. Rowell, J. Noel, and D. Houghton, "Well-resolved band-edge photoluminescence of excitons confined in strained Si_{1-x}Ge_x quantum wells," *Phys. Rev. Lett.*, vol. 66, p. 1362,
- [36] V. Venkataraman, *Physics and applications of Si/Si_{1-x}Ge_x modulation doped structure*. Princeton University, Ph.D. thesis, 1994. Chap. 4.
- [37] D. B. Noble, J. L. Hoyt, C. A. King, J. F. Gibbons, T. I. Kamins, and M. P. Scott, "Reduction in misfit dislocation density by the selective growth of Si_{1-x}Ge_x/Si in small areas," *Appl. Phys. Lett.*, vol. 56, p. 51, 1990.
- [38] E. A. Fitzgerald, Y. H. Xie, D. Brasen, M. L. Green, J. Michel, P. E. Freeland, and B. E. Weir, "Elimination of dislocation in heteroepitaxial MBE and RTCVD Si_{1-x}Ge_x grown on patterned Si substrates," *J. Electrochem. Soc.*, vol. 19, p. 949, 1990
- [39] C. G. Tuppen, C. J. Gibbings, and M. Hockly, "The effects of misfit dislocation nucleation and propagation on Si/Si_{1-x}Ge_x critical thickness values," *J. Growth*, vol. 94, p. 392, 1989.
- [40] E. A. Fitzgerald, G. P. Waston, R. E. Proano, D. G. Ast, P. D. Kirchner, G. D. Pettit, and J. M. Woodall, "Nucleation mechanism and the elimination

- of misfit dislocations at mismatched interface by reduction in growth area," *J. Appl. Phys.*, vol. 65, p. 2220, 1989.
- [41] C. I. Drowley, G. A. Reid, and R. Hull, "Model for facet and sidewall defect formation during selective epitaxial growth of (001) silicon," *Appl. Phys. Lett.*, vol. 52, p. 546, 1988.
- [42] G. Abstreiter, H. Brugger, T. Wolf, H. Jorke, and H. Herzog, "Strain-induced two-dimensional electron gas in selectively doped Si/Si_xGe_{1-x} superlattices," *Phys. Rev. Lett.*, vol. 54, p. 2441, 1985.
- [43] Y. Mii, Y. Xie, E. Fitzgerald, D. Monroe, F. Thiel, B. Weir, and L. Feldman, "Extremely high electron mobility in Si/GeSi structures grown by molecular beam epitaxy," *Appl. Phys. Lett.*, vol. 59, p. 1611, 1991.
- [44] S. Nelson, K. Ismail, J. Nocera, F. Fang, E. Mendez, J. Chu, and B. Meyerson, "Observation of the fractional quantum Hall effect in Si/SiGe heterostructures," *Appl. Phys. Lett.*, vol. 61, p. 64, 1992.
- [45] J. W. Matthews and A. E. Blakeslee, "Defect in epitaxial multilayer structures - I," *J. Cryst. Growth*, vol. 27, p. 118, 1974.
- [46] H. Jorke and H. Herzog, "Mobility enhancement in modulation-doped Si/Si_xGe_{1-x} superlattices grown by MBE," *Proc. of First International Symposium on Molecular Beam Epitaxy*, vol. I, p. 352, 1985.
- [47] E. Fitzgerald, Y.-H. Xie, M. L. Green, D. B. Brason, J. M. A. R. Kortan, Y. J. Mii, and B. E. Weir, "Totally relaxed Si_{1-x}Ge_x layers with low threading dislocation densities grown on Si substrates," *Appl. Phys. Lett.*, vol. 59, p. 811, 1991.

- [48] E. A. Fitzgerald, "The effect of substrate growth area on misfit and threading dislocation densities in mismatched heterostructures," *J. Vac. Sci. Technol. B*, vol. 7, p. 782, 1989.
- [49] V. Venkataraman, C. W. Liu, , and J. C. Sturm, "High mobility electron gases and modulation doped field effect transistors fabricated in Si/SiGe by rapid thermal chemical vapor deposition," *J. Vac. Sci. Technol. B*, vol. 11, p. 1176, 1993.
- [50] A. Krist, D. Godbey, and N. Green, "Selective removal of a $\text{Si}_{0.7}\text{Ge}_{0.3}$ layer from Si(100)," *Appl. Phys. Lett.*, vol. 58, p. 1899, 1991.
- [51] F.K. LeGoues, B. Meyerson, and J. Morar, "Anamolous strain relaxation in SiGe thin films and superlattices," *Phys. Rev. Lett.*, vol. 66, p. 2903, 1991
- [52] D. Dutartre, P. Warren, P. Provenier, F. Chollet, and A. Perio, "Fabrication of relaxed $\text{Si}_{1-x}\text{Ge}_x$ layers on Si substrates by RTCVD," *J. Vac. Sci. Technol. B*, to be published in 1994.
- [53] R. Hull, R. E. Leibenguth, and D. J. Werder, "Role of strained layer superlattice in misfit dislocation reduction in growth of epitaxial $\text{Si}_{0.5}\text{Ge}_{0.5}$ alloys on Si (100) substrates," *J. Appl. Phys.*, vol. 65, p. 4273, 1989.
- [54] Z. Matutinovic-Krstelj, C. Liu, X. Xiao, and J. Sturm, "Evidence of phonon-absorption-assisted electron resonant tunneling si si/ $\text{Si}_{1-x}\text{Ge}_x$ diodes," *J. Vac. Sci. Technol. B*, vol. 11, p. 1145, 1993.
- [55] V. Venkataraman, C. W. Liu, , and J. C. Sturm, "Alloy scattering limited transport of two dimensional carriers in strained $\text{Si}_{1-x}\text{Ge}_x$ quantum wells," *Appl. Phys. Lett.*, vol. 63, p. 2795, 1993.

- [56] V. Venkataraman, C. Liu, and J. Sturm, "High mobility electron gases and modulation-doped field effect transistors fabricated in Si/SiGe by rapid thermal chemical vapor deposition," *J. Vac. Sci. Technol. B*, vol. 11, p. 1176, 1993.
- [57] S. Murphy, Z. Schlesinger, S. F. Nelson, J. O. Chu, and B. S. Meyerson, "Electron cyclotron resonance in silicon/silicon germanium heterostructures," *Appl. Phys. Lett.*, vol. 63, p. 222, 1993.
- [58] C. Kittel, *Introduction to Solid State Physics*. John Wiley, New York, N. Y., 1980. p196.
- [59] D. Lang, R. People, J. Bean, and A. Sergent, "Measurement of the band gap of $\text{Ge}_x\text{Si}_{1-x}/\text{Si}$ strained-layer heterostructures," *Appl. Phys. Lett.*, vol. 47, p. 1333, 1985.
- [60] R. Hull, J. C. Beam, L. Peticolas, and Bahnck, "Growth of $\text{Si}_{1-x}\text{Ge}_x$ alloys on Si (110) surface," *Appl. Phys. Lett.*, vol. 59, p. 964, 1991
- [61] C. Lee and K. L. Wang, "Intersubband absorption in Sb- δ doped Si/Si $_{1-x}$ Ge $_x$ quantum well grown on Si (110)," *Appl. Phys. Lett.*, vol. 60, p. 2264, 1992.
- [62] S. Fukatsu, N. Usami, and Y. Shiraki, "Luminescence from strained Si/Si $_{1-x}$ Ge $_x$ quantum well by molecular beam epitaxy," *Jpn J. Appl. Phys*, vol. 32, p. 2264, 1992.
- [63] J. Sturm, X. Xiao, P. V. Schwartz, C. Liu, L. Lenchyshyn, and M. Thewalt, "Band-edge exciton luminescence from Si/ strained Si $_{1-x}$ Ge $_x$ /Si," *J. Vac. Sci. Technol. B*, vol. 10, p. 1988, 1992.

- [64] X. Xiao, C. Liu, J. Sturm, L. Lenchyshyn, M. Thewalt, R. B. Gregory, and P. Fejes, "Quantum confinement effects in strained silicon-germanium alloy," *Appl. Phys. Lett.*, vol. 60, p. 2135, 1992.
- [65] D. J. Robbins, L. T. Canham, S. J. Barnett, A. D. Pitt, and P. Calcott, "Near-band-gap photoluminescence from pseudomorphic $\text{Si}_{1-x}\text{Ge}_x$ single layers on Si," *J. Appl. Phys.*, vol. 71, p. 1407, 1992.
- [66] J. Weber and M. Alonso, "Near-band-edge photoluminescence of Si-Ge alloys," *Phys. Rev. B*, vol. 40, p. 5683, 1989.
- [67] B. Ridley, *Quantum processes in semiconductors*. Oxford University Press, New York, 1982.
- [68] S. M. Sze, ed., *Physics of semiconductor devices*. John Wiley, New York, NY, 1981. p.13.
- [69] S. H. Li, J. Hinckley, J. Singh, and P. Bhattachary, "Velocity field characterization and alloy scattering in $\text{Si}_{1-x}\text{Ge}_x$," *Electronic Materials Conference*, 1993. Santa Barbara, June.
- [70] G. Bastard, *Wave mechanics applied to semiconductor heterostructures*. Halsted Press, New York, NY, 1988. Chap. 6.
- [71] R. People, J. C. Bean, and D. V. Lang, "Substrate orientation effects on band alignments for pseudomorphic Ge/Si alloy on silicon," *18th International Conference on the Physics of Semiconductors*, vol. I, p. 767, 1986.
- [72] T. Pearsall, ed., *Semiconductor and Semimetals, Vol.32, Strained-Layer Superlattice: Physics*. Academic, New York, NY, 1990. p.141.

- [73] S. Nakamura, T. Mukai, and M. Senoh, "Candela-class high-brightness In-GaN/AlGaIn double-heterostructure blue-light-emitting diodes," *Appl. Phys. Lett.*, vol. 64, p. 1687, 1994.
- [74] V. I. Levin, Y. M. Tairov, M. G. Travazhdyan, V. F. Tsvetkov, and M. A. Chernov, "Study of the growing of silicon carbide single crystal ingots from gas phase," *Sov. Phys. Izvestia*, vol. 14, p. 830, 1978.
- [75] Y. M. Tairov and V. F. Tsvetkov, "Investigation of the growth process of ingots of silicon carbide single crystals," *J. Cryst. Growth*, vol. 43, p. 209, 1978.
- [76] Y. M. Tairov and V. F. Tsvetkov, "General principles of growing large-size single crystals of various silicon carbide polytypes," *J. Cryst. Growth*, vol. 52, p. 146, 1981.
- [77] P. Liaw, , and R. F. Davis, "Epitaxial growth and characterization of β SiC thin film," *J. Electrochem. Soc.*, vol. 132, p. 642, 1985.
- [78] S. Nishino, Y. Hazuki, H. Matsunami, , and T. Tanaka, "Chemical vapor deposition of single crystalline β SiC films on silicon substrates with sputtered SiC intermediate layer," *J. Electrochem. Soc.*, vol. 127, p. 2674, 1980.
- [79] S. Nishino, J. A. Powell, and H. A. Will, "Production of large area single crystal wafers of 3c SiC for semiconductor devices," *Appl. Phys. Lett.*, vol. 42, p. 460, 1983.
- [80] D. E. Ioannou, N. A. Papanicolaou, and P. E. Nordquist, "The effect of heat treatment on Au Schottky contacts on β SiC," *IEEE Trans. Electron Devices*, vol. 34, p. 1694, 1987.

- [81] I. Golecki, F. Reidinger, and J. Marti, "Single crystalline, epitaxial cubic SiC grown on (100) Si at 750 °C by chemical vapor deposition," *Appl. Phys. Lett.*, vol. 60, p. 1703, 1992.
- [82] J. P. Li, J. Steckl, I. Golecki, and F. Reidinger, "Structural characterization of nanometer SiC grown on Si," *Appl. Phys. Lett.*, vol. 62, p. 3135, 1993.
- [83] Z. C. Feng, A. J. Mascarenhas, W. J. Choyke, and P. A. Powell, "Raman scattering studies of chemical-vapor-deposited cubic SiC films of (100) Si," *J. Appl. Phys.*, vol. 64, p. 3176, 1988.
- [84] J. A. Freitas, S. G. Bishop, P. E. R. Nordquist, and M. L. Gipe, "Donor binding energies determined from temperature dependence of photoluminescence spectra in undoped and aluminum-doped β SiC films," *Appl. Phys. Lett.*, vol. 52, p. 1695, 1988.
- [85] R. F. Davis, G. Kelner, M. Shur, J. Palmour, and T. A. Edmond, "Thin film deposition and microelectronic and optoelectronic device fabrication and characterization in monocrystalline α and β silicon carbide," *Proc. IEEE*, vol. 79, p. 677, 1982.
- [86] H. J. Kim, , and R. F. Davis, "Theoretical and empirical studies of impurity incorporation into β SiC thin film during epitaxial growth," *J. Electrochem. Soc.*, vol. 133, p. 2350, 1986.
- [87] N. A. Papanicolaou, A. Christou, and M. L. Gipe, "Pt and PtSi_x Schottky contacts on n-type β SiC," *J. Appl. Phys.*, vol. 65, p. 3526, 1989.
- [88] M. Bhatnagar and B. J. Baliga, "Comparison of 6H-SiC, 3C-SiC, and Si for power devices," *IEEE Trans. Electron Devices*, vol. 40, p. 645, 1993.

- [89] P. G. Neudeck, D. J. Larkin, J. E. Star, J. A. Powell, C. S. Salupo, and L. G. Matus, "Greatly improved 3C-SiC p-n junction diodes grown by chemical vapor deposition," *IEEE Electron Device Lett.*, vol. 14, p. 136, 1993.
- Sze, *Physics of semiconductor devices*. John Wiley, New York, NY, 1981.
- Sze, *Semiconductor Devices: physics and technology*. John Wiley, New York, N. Y., 1985. p 66.
- [92] M. Bhatnagar, P. K. Mclarty, and B. J. Baliga, "Silicon carbide high voltage (400 V) Schottky barrier diodes," *IEEE Electron Device Lett.*, vol. 13, p. 501, 1992.
- [93] T. K. Ning and D. D. Tang, "Bipolar trend," *Proc IEEE*, vol. 74, p. 1669, 1986.
- [94] T. Sugii, T. T. Ito, Y. Furumura, M. Doki, F. Mieno, and M. Maeda, " β SiC heterojunction bipolar transistors with high current gain," *IEEE Electron Device Lett.*, vol. 9, p. 87, 1988.
- [95] E. J. Prinz, *Base transport and vertical profile engineering in Si/Si_{1-x}Ge_x/Si heterojunction bipolar transistors*. PhD thesis, Princeton University, 1993.
- [96] R. A. Soref, "Optical bandgap of the ternary semiconductor Si_{1-x-y}Ge_xC_y," *J. Appl. Phys.*, vol. 70, p. 2470, 1991.
- [97] J. L. Regolini, F. Gisbert, G. Dolino, and P. Boucaud, "Growth and characterization of strain compensated Si_{1-x-y}Ge_xC_y epitaxial layers," *Materials Lett.*, vol. 18, p. 57, 1993.
- [98] K. Elbert, S. S. Iyer, S. Zollner, J. C. Tsang, and F. K. LeGoues, "Growth and strain compensation effects in the ternary Si_{1-x-y}Ge_xC_y alloy system," *Appl. Phys. Lett.*, vol. 60, p. 3033, 1992.

- [99] S. Im, J. Washburn, R. Gronsky, N. W. Cheung, K. M. Yu, and J. W. Ager, "Optimization of Ge/C ratio for compensation of misfit strain in solid phase epitaxial growth of SiGe layers," *Appl. Phys. Lett.*, vol. 63, p. 2682, 1994.
- [100] P. Boucaud, C. Francic, F. H. Julien, J. M. Lourtioz, D. Bouchier, S. Bodnar, B. Lambert, and J. L. Regolini, "Band gap and deep level photoluminescence of pseudomorphic $\text{Si}_{1-x-y}\text{Ge}_x\text{C}_y$ alloy," *Appl. Phys. Lett.*, vol. 64, p. 875, 1994.
- [101] K. Elbert, S. S. Iyer, J. C. Tsang, M. S. Goorsky, and F. K. LeGoues, "The growth and characterization of $\text{Si}_{1-y}\text{C}_y$ alloy on Si(001) substrate," *J. Vac. Sci. Technol. B*, vol. 10, p. 934, 1992.
- [102] T. Fukazawa, K. Sasaki, and S. Furukawa, "Preparation of microcrystalline silicon carbide thin films for the emitter of Si hbt," *Amorphous and Crystalline Silicon Carbide II, Proc. of the 2nd International Conference, Santa Clara, C. A.*, p. 49, 1988.
- [103] R. Zachai, K. Ebert, and G. Abstreiter, "Photoluminescence in short-period Si/Ge strained layer superlattice," *Phys. Rev. Lett.*, vol. 64, p. 1055, 1990.

Processing Notes for Negative Photoresist

The square pattern of oxide hole on Si substrates (chapter 2) was defined by negative photoresist, which is not commonly used in the lithography process. For the convenience of future reference, the recipe of 747 negative photoresist with the viscosity of 60 cs is provided :

1. Dehydration: After the oxidized Si wafers are cleaned, the wafers should be baked at 120 °C to remove water vapor.
2. Coating: After being spin-coated with HMDS (optional), the wafers can be spin-coated with negative photoresist using the spin speed of 4000 rpm to obtain a thickness of about 1 μm .
3. Cure: A soft bake at 90 °C for 10 min is preferred.
4. Exposure: For the light intensity (5mW/cm²) of the mask aligner in Prof. Tsui's clean room, the exposure time is about 1 second.
5. Develop/Rinse: This process is similar to that of positive photoresist. But the develop is "Projection Develop", and the N-Butyl Rinse is used (not water).
6. Post Bake: A post bake at 120 °C for 20 min is required.
7. Descum: Because the negative photoresist is clear, an oxygen plasma (5min at 50 Watts) is used to remove the residual photoresist.

8. Strip: Hot acid (sulfuric acid with hydrogen peroxide) or J-1000 stripper is used to remove the photoresist after the pattern is defined.

9. For selective growth, the wafer should be cleaned again by RCA cleaning. The clean wafer is required to ensure the selectivity of epilayers and to avoid the contamination of the reactor.

Appendix B

Log-book of Typical Samples Used in This Study

This is a summary of growth steps of typical samples used in this study. A cleaning step consisting of a 2 min bake at 1000°C 250 torr followed by a high temperature buffer was performed on all samples prior to designed layer structures.

Sample #702

Selective epitaxial growth (chapter 2).

time min	temp °C& slpm	H ₂ sccm	DCS sccm	GeH ₄ sccm	thickness Å	description
2	1000		4			cleaning
0.5	900	3	26		700	buffer
40	625	3	26	41	2000	Si _{0.87} Ge _{0.13}
1	700	3	26		30	Si cap

Sample #1341

Grade relaxed buffer with a modulation doped structure (chapter 3). The cleaning step was the same as sample 702. The high temperature buffer was grown at 1000 °C with the thickness of 2 μm by DCS flow of 26 sccm.

time min	temp °C	DCS sccm	GeH ₄ sccm	PH ₃ sccm	thickness Å	description
50	625	26	0-31		1000	0-10% grading
40	625	26	31-100		2500	10-20% grading
13	625	26	100-450		2600	30-38% grading
20	625	26	450		6000	uniform Si _{0.62} Ge _{0.38} layer
60	800					anneal relaxed buffer at 6 torr
2.5	700	26			75	strained Si channel
20sec	625	26	450		100	spacer
55sec	625	26	450	100	300	doped supply and cap layer

Sample #1463

Si/Si_{0.71}Ge_{0.29}/Si quantum wells on < 110 > Si substrates (chapter 4).

time min	temp °C	H ₂ slpm	DCS sccm	GeH ₄ sccm	thickness Å	description
2	1000	4				cleaning
10	1000	3	26		2 μm	buffer
1	1000	3	26		30	buffer II
	625	3	26	450	51	Si _{0.71} Ge _{0.29} layer
6	700	3	26		100	Si cap

Sample #1221

Schottky barriers on boron compensated n-type SiC (chapter 5).

time min	temp °C	H ₂ slpm	SiCH ₄ sccm	DCS sccm	B ₂ H ₂ sccm	thickness Å	description
2	1000	4					cleaning
10	1000	3		26		2 μm	buffer(n-type)
1	1000	3		26		30	buffer II
30	800	0.24	1.5		250	0.45 μm	n-SiC, Pressure= 1torr

Sample #1603

SiGeC alloys grown by DCS (chapter 6). Details of the growth program is given in Appendix C.

time min	temp °C	H ₂ slpm	SiCH ₄ sccm	DCS sccm	GeH ₄ sccm	SiH ₄ sccm	thickness Å	description
2	1000	4						cleaning
10	1000	3		26			2 μm	buffer(n-type)
1	1000	3		26			30	buffer II
10	550	3	0.15	26	100		60	SiGeC
30	550	3				100	50	Si cap

C. Growth sequence of sample #1603

123

4	SET(DO1,1)	H2 on
5	WAITUNTIL(AI29>0.25)	pressuring chamber
6		
7		
8	RAMP(SP7,0.4,0.274)	T 1000°C
9	WAIT(120)	cleaning
10	SET(AO8,0.0)	
11	SET(AO0,0.617)	H2 flow 3 slpm
12		
13		
14	WAITUNTIL(AI29<0.01)	pump out
15	WAITUNTIL(AI24>0.5)	open valve, go for buffer
16	SET(AO11,1)	sel low pressure
17	WAITUNTIL(AI29<0.5)	pump out
18	SET(AO6,0.6)	P 6 torr
19		
20	WAIT(30)	stablize pressure, flow
21	SET(DO13,1)	DCS inj
22	WAIT(600)	growing buffer
24	SET(SP2,1.0)	done

Sequencer Table # 5

<u>Step</u>	<u>Action</u>	<u>Comment</u>
0	RAMP(SP7,-0.4,0.0)	lamp down to zero
1		
2		

3	WAITUNTIL(AI24>0.5)	Check T control, Go for cold value
4	SET(SP3,1.0)	
5	WAIT(1)	
6	SET(SP3,0.0)	
7		
8	RAMP(SP7,0.4,0.274)	lamp up to 27.4%
9	SET(DO13,1)	inj DCS
10	WAIT(60)	Buffer II
11	RAMP(SP7,-0.4,0.133)	lamp down to 13.3 %
12	SET(DO2,1)	SiH4 sel on
13	SET(SP5,1.62)	T 550 °C
14	SET(SP4,1)	feedback on
15	SET(DO3,1)	sel GeH4
16	SET(DO13,0)	DCS inj off
17	SET(DO8,1)	SiCH6 sel
18	WAIT(180)	stabilize flow
19	SET(SP2,1)	
20	END	

Sequencer Table # 3

<u>Step</u>	<u>Action</u>	<u>Comment</u>
0	SET(DO13,1)&	DCS SiCH6 inj
1	SET(DO10,1)	inj Germane
2	WAIT(600)	SiGeC growth
3	SET(DO13,0)&	DCS SiCH4 off
4	SET(DO10,0)	GeH4 inj off

C. Growth sequence of sample #1603

125

5	WAIT(20)	
6	SET(DO9,1)	SiH4 inj on
7	WAIT(1800)	Si Cap,turn of GeH4 sel manually
8	SET(DO9,0)	SiH4 inj Off
9	WAIT(20)	
10	SET(DO8,0)	SiH4 sel off
11		
12	SET(SP7,0.0)	lamp off
13	SET(SP4,0.0)	
14	SET(SP2,1)	
15	END	

Sequencer Table # 7

<u>Step</u>	<u>Action</u>	<u>Comment</u>
0	SET(SP7,0)&	lamp off
1	SET(DO13,0)	
2	SET(DO12,0)	
3	SET(DO11,0)	
4	SET(DO9,0)	
5	SET(DO7,0)	
6	SET(DO6,0.0)	
7	SET(DO5,0)	
8	SET(DO4,0)	
9	SET(DO3,0)	
10	SET(DO2,0)	
11	SET(DO1,0)	

C. Growth sequence of sample #1603

126

12	SET(AO8,0)	
13	SET(AO7,0)	
14	SET(AO6,0)	
15	SET(AO5,0)	
16	SET(AO4,0)	
17	SET(AO3,0)	
18	SET(AO2,0)	
19	SET(AO1,0)	
20	SET(AO8,0)	
21	WAITUNTIL(AI28<0.5)	
22	SET(DO15,0)	vacuum off
23	SET(DO8,0)	
24	SEQUENCE OFF (0)	
25	SEQUENCE OFF (1)	
26	SEQUENCE OFF (2)	
27	SEQUENCE OFF (3)	
28	SEQUENCE OFF (4)	
29	SEQUENCE OFF (5)	
30	SEQUENCE OFF (6)	
31	SEQUENCE OFF (7)	

Sample List of SiGeC Alloys

The following tables summarize the samples used in the SiGeC study. Table D.1 gives the samples by DCS growth. Table D.2 gives the samples by silane growth. The RBS measurement was performed by Dr. N. Moriya of AT&T Bell Labs. The TEM was performed by Dr. Dave Eaglesham of AT&T Bell Labs. PL measurement at 30K was obtained by Yves R. J. Lacroix. Some of the samples were grown by Anthony St. Amour in our lab.

Sample #	SiCH ₄ flow/time (sccm/min)	Si Cap temp./time (°C /min)	IR type	X-ray	PL good (temp.)	RBS Ge cm ⁻²
1592	0.25/50	600/4	substitutional C	single cryst.	no	
1590	0.9/50	600/4	poly SiC		no	
1591	1.5/50	550/20	amorphous SiC		no	
1584	12/50	none	poly SiC		no	
1601	0.5/100	none		amorphous		
1602	0/10(60Å)	550/40			77, 30 K	7.36E15
1603	0.15/10(60Å)	550/30			77, 30 K	7.13E15
1607	0.23/10(60Å)	550/30			77, 30 K	8.10E15
1612	0.23/100	550/30		[C] = 0.8%	no	4.37E16
1613	0.15/100	550/30		[C] = 1.6%	no	5.85E16
1614	0/100	550/30		[Ge] = 0.25%	no	5.27E16

Table D.1: Summary of SiGeC alloys by DCS growth. The SiGeC alloys were grown at 550 °C with DCS flow of 26 sccm, germane mixture (0.8% in hydrogen) flow of 100 sccm and various methylsilane flows. The Si cap was grown by silane mixture (4% in hydrogen) flow of 100 sccm with various temperature and growth time. The growth pressure was 6 torr for all the layers. The thicknesses of sample 1602, 1603 and 1607 were obtained by XTEM.

Sample #	SiCH ₄ flow/time (sccm/min)	Si Cap temp./time (°C /min)	IR type	X-ray	PL good (temp.)	RBS Ge cm ⁻²
1597	0/50	none		[Ge] = 0.22%		
1593	0.1/50	600/4	substitutional C	[C] = 0.1%	no	
1598	0.2/50	none		amorphous		
1599	0.3/50	none				
1594	0.5/50	none	amorphous SiC	amorphous		
1586	0.8/50	none	amorphous SiC	amorphous		

Table D.2: Summary of SiGeC alloys by Silane growth. The SiGeC alloys were grown at 550 °C with silane mixture (4% in hydrogen) flow of 50 sccm, germane mixture (0.8% in hydrogen) flow of 100sccm and various methylsilane flows. The Si cap was grown by silane mixture (4% in hydrogen) flow of 100 sccm with various temperature and growth time. The growth pressure was 6 torr for all the layers.

Publications and Presentations Resulting from This Work

A: JOURNAL PAPERS

1. C. W. Liu and J. C. Sturm, "60-V Reverse Hard Breakdown SiC Schottky Barriers on (100) Si," in preparation.
2. C. W. Liu, J. C. Sturm, Y. Lacroix, M. L. W Thewalt, and D. D. Perovic "Growth and Bandgap of Strained $\langle 110 \rangle$ $\text{Si}_{1-x}\text{Ge}_x$ Layers on Silicon Substrates by Chemical Vapor Deposition," *Appl. Phys. Lett.*, vol. 65(1), pp. 1-3, 1994
3. J. C. Sturm, X. Xiao, Q. Mi, C.W. Liu, A. St Amour, Ž. Matutinović-Krstelj, L. C. Lenchyshyn, and M. L. W Thewalt, "Photoluminescence and Electroluminescence process in $\text{Si}_{1-x}\text{Ge}_x/\text{Si}$ Heterojunction Grown by Chemical Vapor Deposition," *Mater. Sci. Eng.B21*, pp. 307-311, 1993
4. V. Venkataraman, C. W. Liu and J. C. Sturm, "Alloy Scattering Limited Transport of Two-dimensional Carriers in Strained $\text{Si}/\text{Si}_{1-x}\text{Ge}_x$ Quantum Wells," *Appl. Phys. Lett.*, vol. 63(20), pp. 2795-2797, 1993.
5. P. V. Schwartz, C. W. Liu, and J. C. Sturm, "Semi-insulating Crystalline Silicon Formed by Oxygen Doping During Low-temperature Chemical Vapor Deposition," *Appl. Phys. Lett.* , vol. 62(10), pp. 1102-1104, 1993.

6. Ž. Matutinović-Krstelj, C. W. Liu, X. X. Xiao, and J. C. Sturm, "Symmetric Si/Si_{1-x}Ge_x Electron Resonant Tunneling Diodes with an Anomalous Temperature Behavior," *Appl. Phys. Lett.*, vol. 62(6), pp. 603–605, 1993.
7. V. Venkataraman, C. W. Liu and, J. C. Sturm, "High Mobility Electron Gases with Very Low Sheet Resistivities and MODFETs Fabricated in Si/Si_{1-x}Ge_x ," *J. Vac. Sci. Technol. B.* vol. 11(3), pp.1176-1178, 1993.
8. Ž. Matutinović-Krstelj, C. W. Liu, X. Xiao and J. C. Sturm, "Electron Si/SiGe Resonant Tunneling Diode Grown by RTCVD, " *J. Vac. Sci. Technol. B.* vol. 11(3), pp.1145-1148, 1993.
9. (Invited) J. C. Sturm, X. Xiao, P. V. Schwartz, C. W. Liu, L. C. Lenchyshyn, and M. L. W Thewalt, "Band-edge Exciton Luminescence from Si/ strained Si_{1-x}Ge_x/Si," *J. Vac. Sci. Technol. B.*, vol. 10(4), pp. 1998–2001, 1992.
10. X. Xiao, C. W. Liu, J. C. Sturm, L. C. Lenchyshyn, M. L. W Thewalt, R. B. Gregory, and P. Fejes, "Quantum Confinement Effects in Strained Silicon-Germanium Alloy Quantum Wells," *Appl. Phys. Lett.* vol. 60(17), pp. 2135–2137, 1992.
11. X. Xiao, C. W. Liu, J. C. Sturm, L. C. Lenchyshyn, and M. L. W Thewalt, "Photoluminescence from Electron-hole Plasma Confined in Si/Si_{1-x}Ge_x/Si Quantum Wells," *Appl. Phys. Lett.*, vol. 60(14), pp. 1720–1722, 1992.

B: REFEREED CONFERENCE PAPER and PRESENTATION

1. C. W. Liu, A. St. Amour, and J. C. Sturm, "Low Temperature Chemical Vapor Deposition of SiGeC Alloys on (100) Si Substrates," accepted by *Electronic Materials Conference*, 1994; to be published in *J. Electronic Material*.
2. C. W. Liu, J. C. Sturm, Y. Lacroix, and M. L. W Thewalt, "Growth and Photoluminescence of Strained (110) Si/Si_{1-x}Ge_x/Si Quantum Wells Grown by Rapid Thermal Chemical Vapor Deposition," *Proc. Symp. Mat. Res. Soc.*, vol. 342, 1994.
3. C. W. Liu and J. C. Sturm, "Growth of Low-temperature SiC on Tilted and Not-tilted (100) Si with 60-V Breakdown Schottky Barriers," Proceedings of 5th International Conference of SiC and Related Materials, Washington D. C., 1993; To be published in the international Institute of Physics Conference Series.
4. C. W. Liu, J. C. Sturm, and E.A. Fitzgerald, "Structural and Electrical Characteristics of Low-temperature Cubic SiC on (100) Si," *Electronic Materials Conference*, Santa Barbara CA, 1993; *J. Electronic Material*, vol. 22(7A), pp. A41, 1993.
5. V. Venkataraman, C. W. Liu, and J. C. Sturm, "Effect of Alloy Scattering on Low Temperature Mobilities of Two-dimensional Holes and Electrons in Si/Si_{1-x}Ge_x Heterstructures," *Electronic Materials Conference*, Santa Barbara CA, 1993; *J. Electronic Material*, vol. 22(7A), pp. A19, 1993.
6. C. W. Liu, J. C. Sturm, P. V. Schwartz and E. A. Fitzgerald, "Misfit Dislocation Nucleation Sites and Metastability Enhancement of Selective Si_{1-x}Ge_x Grown by Rapid Thermal Chemical Vapor Deposition," *Proc. Symp. Mat. Res. Soc.*, vol. 238, pp.85-90, 1992.

7. **P. V. Schwartz, C. W. Liu, J. C. Sturm, T. Gong and P. M. Fauchet, "Current Transport Properties of Semi-Insulating Oxygen-Doped Silicon Films for Use in High Speed Photoconductive Switch," *Electronic Materials Conference*, Boston, MA, 1992.

** Best Student Paper Award, *Electronic Materials Conference*, Boston, MA, 1992.
8. P. V. Schwartz, C. W. Liu, and J. C. Sturm, "Oxygen-doped Semi-insulating Epitaxial Silicon Grown by Low-Temperature Thermal Chemical Vapor Deposition," *Technical Program, 23rd IEEE Semiconductor Interface Specialist Conference*, San Diego, CA, 1992.
9. V. Venkataraman, C. W. Liu, and J. C. Sturm, "High Mobility Electron Gases with Very Low Sheet Resistivities and MODFETs Fabricated in Si/Si_{1-x}Ge_x by Rapid Thermal Chemical Vapor Deposition," 39th National Symp. of American Soc., 1992.
10. Ž. Matutinović-Krstelj, C. W. Liu, X. X. Xiao, and J. C. Sturm, "Electron Si/SiGe Resonant Tunneling Diode Grown by RTCVD," 39th National Symp. of American Vac. Soc., 1992.